DOI 10.1515/nanoph-2013-0001 — Nanophotonics 2013; aop

Vijay Kris Narasimhan and Yi Cui*

Nanostructures for photon management in solar cells

Abstract: The concurrent development of high-performance materials, new device and system architectures, and nanofabrication processes has driven widespread research and development in the field of nanostructures for photon management in photovoltaics. The fundamental goals of photon management are to reduce incident light reflection, improve absorption, and tailor the optical properties of a device for use in different types of energy conversion systems. Nanostructures rely on a core set of phenomena to attain these goals, including gradation of the refractive index, coupling to waveguide modes through surface structuring, and modification of the photonic band structure of a device. In this review, we present recent developments in the field of nanostructures for photon management in solar cells with applications across different materials and system architectures. We focus both on theoretical and numerical studies and on progress in fabricating solar cells containing photonic nanostructures. We show that nanoscale light management structures have yielded real efficiency gains in many types of photovoltaic devices; however, we note that important work remains to ensure that improved optical performance does not come at the expense of poor electrical properties.

Keywords: photon management; nanostructures; graded index; grating; guided mode; photonic crystal; solar cell.

***Corresponding author: Yi Cui,** Department of Materials Science and Engineering, Stanford University, Stanford, California 94305, USA; and Stanford Institute for Materials and Energy Sciences, SLAC National Accelerator Laboratory, 2575 Sand Hill Road, Menlo Park, CA 94025, USA, e-mail: yicui@stanford.edu
Vijay Kris Narasimhan: Department of Materials Science and Engineering, Stanford University, Stanford, CA 94305, USA

1 Introduction

The prospect of the widespread adoption of solar energy generation from photovoltaics is in reach. Continuous improvement in materials quality and cell design and scaling of manufacturing have led to better efficiency [1] and reduced cost [2] in many types of solar cells, with both silicon and cadmium telluride module costs dropping to below $1/W. Coupling as much light as possible into solar cells is important in achieving both goals, and therefore current solar cells incorporate light management elements, including antireflection coatings, back-reflectors, and surface texturing, to reduce optical losses.

There is also a trend across many solar cell technologies towards thinner devices. The reasons for reducing the dimensions of the active layer vary by technology, from reducing the weight and thickness of silicon devices to using less scarce material in cadmium telluride and CIGS devices [3] to eliminating light-induced degradation in amorphous silicon devices [4] to improving charge collection efficiency in organic devices [5] to reducing the cost of gallium arsenide devices [6]. Thinner solar cells, while offering numerous advantages, present new challenges to cell designers. A decrease in thickness may also be accompanied by incomplete absorption of photons and a corresponding decrease in efficiency. Moreover, as solar cells make their way into different types of systems and architectures, including tracking systems, concentrator systems, and building-integrated systems, new optical requirements, such as better angular performance, partial transparency or reflectivity, and directional selectivity, emerge.

Thankfully, shrinking the scale of light management elements can meet the demands of these shrinking absorber layers. At the nano and meso scales, new phenomena such as graded index interfaces, strong coupling to guided modes, and photonic bandstructures for spectral and directional selectivity emerge from the physics of Maxwell's equations. In this review, we focus on the rich portfolio of structures that enable these phenomena, namely nanotextured antireflection coatings, surface structures for coupling into waveguides, and photonic crystals.[1] We highlight key developments in theory and experimental processes applicable to the wide variety of material systems and applications under development today.

1 Another important photon management technique, plasmonics, which exploits collective resonant electron oscillations in the free-electron like gasses of particles and surfaces, has been previously reviewed in this journal [7] and elsewhere [8]. We refer the interested reader to those publications

2 Graded Index antireflection layers

2.1 Overview and theory

One of the fundamental goals of photon management in solar cells is to reduce light loss from reflection off the front surface of the cell. Consider a polished silicon solar cell with no antireflection coating; when averaged over the absorbed part of the solar spectrum (up to 1100 nm) and across all incident angles, ~37% of light is lost to reflection. Such high reflection arises from the mismatch in the refractive index between the air and the solar cell. A common way to reduce this loss is through an antireflection layer with a thickness of 0.25λ, where λ is the wavelength of interest. Destructive interference results from the phase difference between light reflected from the top and bottom interfaces of the antireflection layer. However, antireflection coatings are highly wavelength- and angle-specific.

Alternatively, an antireflection layer with an index that varies gradually from that of the air to that of the substrate could be used to reduce the apparent abruptness of the interface [9]. In principle, antireflection effects from such a film would be broadband and quasi-omnidirectional. To be an effective graded index layer, the wavefunction of the incident light must vary slowly through its depth, i.e., the wavelength of the light must be on the same scale as the depth of the graded index layer or smaller. Index matching is also best when the gradient is "flat" at the ultimate interfaces with the air and the substrate, i.e., when the functional form of the gradient profile has multiple continuous derivatives at these interfaces. Nearly ideal continuous graded index profiles include the quintic profile described by Southwell [10] and the half-period of an exponential sine function [11]. Such ideal profiles are difficult to fabricate in practice; however, other non-ideal profiles, such as linear gradients, truncated polynomial gradients, and multi-layer approximations of ideal gradients, can still demonstrate extremely low reflection. Graded index layers can be implemented by nanostructured layers or wavelength scale mesostructures, as described in the following sections.

2.2 Nanostructures

One approach to achieving a high-performance graded index profile is to use nanostructures much smaller than the wavelength of light to vary the density of the material above the active layer of the cell. As the density varies, so too does the effective refractive index of the material. For example, the Schubert group has used a combination of standard thin film growth and oblique-angle deposition to deposit silica and titania multi-layer films. When deposited at oblique angles, nanorod arrays are formed with a reduced refractive index depending on the fill fraction of the layer. The group developed a 5-layer film with a reflection minimum of <0.2% at 632 nm [12]; this structure approximated a modified quintic profile (Figure 1). The group also devised a three layer film optimized for silicon solar cells which outperformed a standard λ/4 antireflection coating, reducing overall reflection to <6% [13]. Recently, the group applied their technique to developing a 4-layer antireflection coating for multi-junction solar cells (i.e., cells that contain a stack of semiconductor junctions with different band gaps connected in series) [14]. They reduced reflections at normal incidence on an inverted metamorphic triple-junction device to 3.9% as compared to 7.9% for an optimized dual-layer antireflection coating on the same device.

Continuous density gradient layers have also been explored. For example, Koynov and colleagues sputtered metal onto crystalline, polycrystalline, and amorphous silicon substrates and performed wet chemical etching to roughen the surface with random hillocks ranging from 10–100 nm in width and up to 250 nm in height [15]. Reflection was reduced to 2–5% in the highly absorptive wavelength ranges of the samples.

Branz and colleagues [16] used a solution of $HAuCl_4$ or ~5 nm colloidal gold nanoparticles, HF, and H_2O_2 to perform a catalyzed etch of interconnected pores in the <1 0 0> directions in silicon. From measurements of

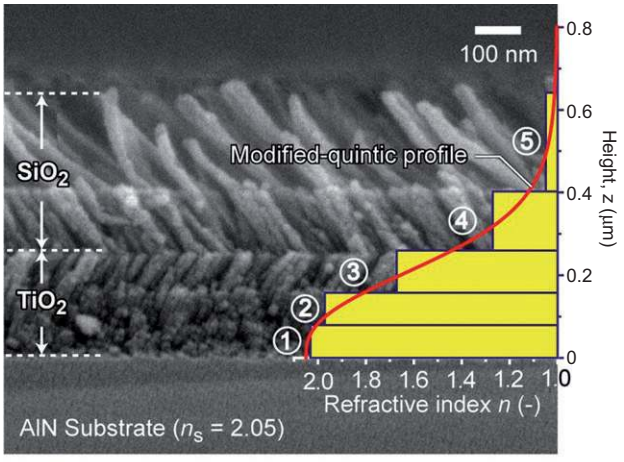

Figure 1 Approximation to a modified quintic profile using oblique angle deposition of nanorod arrays. Used with permission from [12].

reflectance as a function of etch time, they found empirically that reflection falls off exponentially with increasing ratio of the depth of the gradient to the wavelength. They achieved a minimum reflectance of <2% across the spectrum from 300 nm to 1100 nm. Nanoparticle etching can also give rise to a silicon sponge architecture which shows good antireflection performance [17].

Oh and colleagues [18] used a similar fabrication method (silver nanoparticle-assisted etching) to study techniques for improving the conversion efficiency of a silicon solar cell with a graded index layer. In a configuration in which a porous nanostructure occupies a significant volume fraction of the emitter layer (i.e., the n+ layer of the p/n junction), a silicon solar cell typically has a poor absorbed-photon-to-electron conversion efficiency, or internal quantum efficiency, especially in the blue wavelengths (400–600 nm). In lighter doped emitters, surface recombination of photoexcited carriers dominates, whereas Auger recombination is more significant in more heavily doped emitters. Nanostructures exacerbate both types of recombination since they present a large surface area and also enable high dopant concentrations in volumes of the cell with high light absorption. By using a TMAH etch step after dopant diffusion in a silicon cell with a porous graded index layer, the authors simultaneously reduced the surface area and the dopant concentration near the surface and realized an impressive efficiency of 18.2%.

Density variations can also be advantageous in antireflection layers deposited on top of the active layer in a solar cell; in essence, this produces a truncated graded index profile with a continuous gradient from air to the bottom of the antireflection coating and an abrupt discontinuity between the bottom of the antireflection layer and the active layer of the device. Any optical losses from the discontinuity may be compensated by the fact that the solar cell may avoid damage and deteriorated electrical performance associated with patterning the active layer itself.

For example, Lee and colleagues suppressed reflection from a silicon solar cell using a zinc oxide nanoneedle antireflection layer grown by a two-step liquid phase technique [19]. A highly tapered structure, with a height of 1.5 μm, an average tip diameter of 10 nm, and a base diameter of 45 nm, provided the best performance, reducing the weighted reflection to 6.6% across the solar spectrum. 2.6 μm zinc oxide nanoneedles have also been shown to successfully improve the short-circuit current density of a GaAs-based multi-junction solar cell by 16.7% [20]. Preliminary investigations have also been conducted on GaP nanowire grasses for use in multi-junction devices [21].

2.3 Mesostructures

Wavelength-scale mesostructures can also function as effective graded-index coatings. For example, vertically-aligned nanopillar arrays with a moderate filling fraction formed by dry [22, 23] or wet [24] etching substantially reduce reflections owing to the formation of an intermediate refractive index layer between air and the substrate. The performance can be further improved from the step profile created by nanopillars by tapering the structures into nanocones to produce a continuous graded index profile. For example, Yu and colleages [25] devised a technique for forming very regular silicon nanocones by nano-imprinting a pattern on a tri-layer resist, multi-step reactive ion etching to transfer the pattern through the resist, depositing and lifting off metal to create a hard mask, and further reactive ion etching to create the nanocones. Reflectivity of <5% was achieved across the solar spectrum for cones with a lateral period of 200 nm and a height of 520 nm.

In contrast to the complexity of this multi-step process, Huang and colleagues devised a single-step self-masked fabrication process to produce silicon nanotips across a wafer [26]. By adding silane to a standard set of etch gases in a dry-etching machine, a flat silicon substrate was etched while a silicon carbide etch mask was simultaneously formed. This resulted in an array of tapered nanowires of various heights and profiles that suppressed reflection to ~ 1% in the wavelength range of interest.

Our group developed a wafer-scale approach that offers both precise control of the spacing and profile of the nanocones with a simple fabrication process [27]. First, we use Langmuir-Blodgett deposition to coat large areas of a substrate with a close-packed array of silica nanoparticles that act as an etch mask. We also subsequently developed a roll-coating technique that achieves similar coverage [28]. Next, we use dry etching to pattern the substrate. By tuning the dimensions of the starting template and the etching conditions, and therefore the shrinkage of the particles and the undercut during the etch, vertical as well as tapered profiles can be obtained (Figure 2). We showed by comparing the absorption in an amorphous silicon layer that the tapered structure improved absorption compared to a columnar structure fabricated from the same template and a planar film at all wavelengths of interest (Figure 3) [23]. The performance of nanocones at off-normal angles of incidence was also found to be superior to nanopillars and the planar structure.

A similar technique was devised for forming rounded nanocones on gallium arsenide through

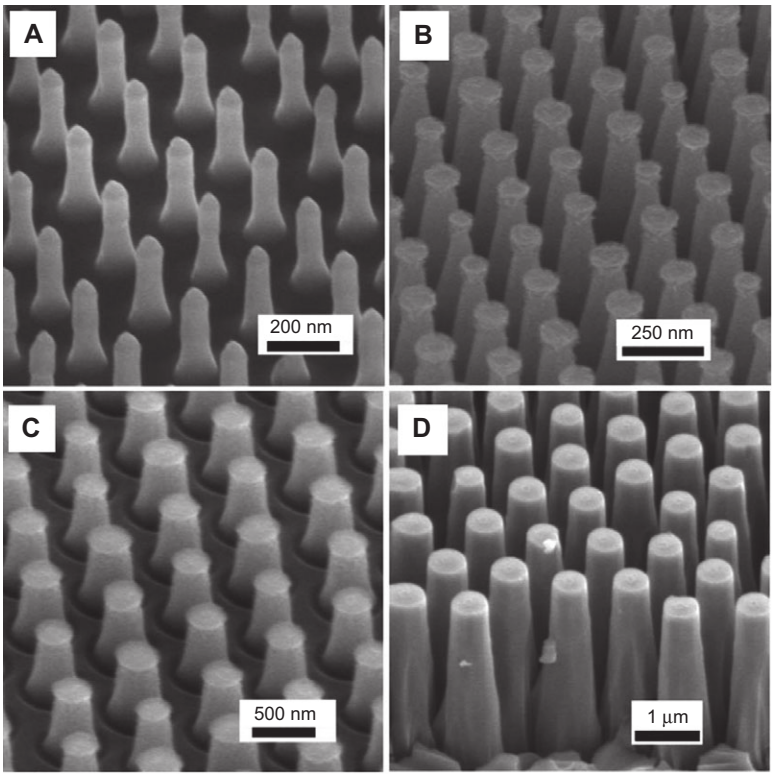

Figure 2 Various etch profiles obtained using a silica nanosphere template and reactive ion etching of silicon substrates. Reused with permission from [27].

holographic lithography, thermal reflow of the photoresist, and dry etching [29]. For GaAs nanocones with 300 nm spacing, reflection was suppressed to <5% in the wavelength range of 300–1100 nm. Interference lithography was used to produce a moth-eye surface texture on organic solar cells which gave rise to a 3.5% improvement in the peak external quantum efficiency of the device. Of note, the current generated from the device improved further at oblique angles up to 50° from normal incidence [30].

Analysis has also been conducted to find optimal antireflection meso structures [31–33]. Findings from these studies confirm some general trends about mesostructures. First, reflection is minimized when the spacing of the mesostructure is on the order of the average wavelength between air and the substrate; as the spacing or

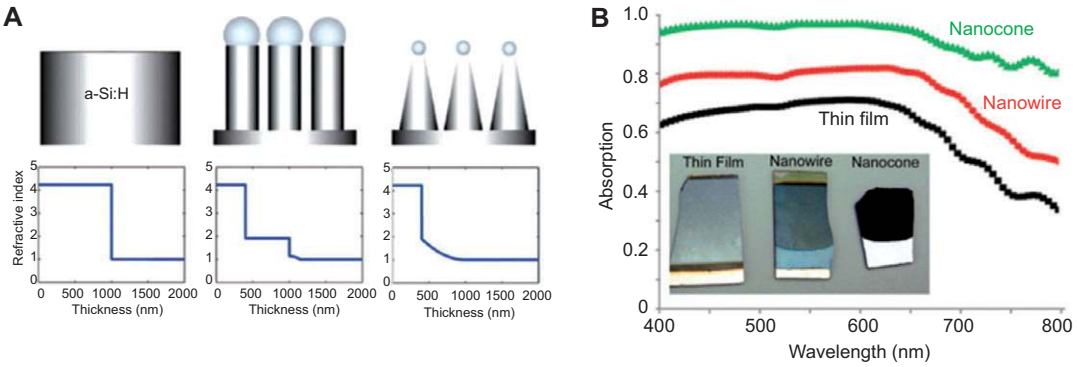

Figure 3 (A) Refractive index profile and (B) absorption spectrum of nanocones, nanowires, and planar amorphous silicon samples (optical photograph shown inset). Adapted with permission from [23], ©2012 American Chemical Society.

period of the mesostructure decreases, the location of the reflection minimum blue-shifts. Second, antireflection generally improves as the ratio of height to spacing in the mesostructure increases; however, if the base of the mesostructure does not tile the substrate completely, i.e., if there are spaces in the structure, then the reflection saturates. Third, structures in which the variation in the effective refractive index (i.e., the gradient profile) is slow at the ultimate air and substrate interfaces outperform structures with a linear gradient profile.

It is worth noting that tapering reduces reflections and promotes coupling into non-planar active layers as well. Using rigorous coupled wave analysis, Alaeian and colleagues found that the absorptance of an array of silicon nanopillars could be improved by capping the cylinders with conical tips with an optimal sidewall angle of 60° [31]. Tapering was also used in germanium nanopillar arrays formed by growth in an anodic aluminum oxide template. Dual-layer nanopillars were formed by varying the diameter of the template from 130 nm in the lower half of the pillar to 60 nm in the upper half of the pillar. The structure demonstrated 99% absorptance in the wavelength range of 300–900 nm, far higher than the absorptance achieved when either 60 or 130 nm pillars were used alone [34].

As was the case for nanoscale structures, mesoscale graded index structures can also be implemented in a specific antireflection layer to avoid patterning the active layer. For example, our group devised a technique to grow tin oxide nanocones by controlled oxidation of tin nanoislands formed after sputtering of thin tin metal films. The absorption in a polycrystalline silicon substrate was improved by 30% in the wavelength range of 400–850 nm owing to the antireflection effect of the nanocones [35]. In another study, etching of nanopillars into the SiO_2 layer of a bilayer SiO_2/TiO_2 antireflection coating produced a ~5% improvement in the output power of a silicon solar cell at normal incidence and a 55.8% improvement at 60° incidence as compared to the power generated from a cell coated with a planar SiO_2/TiO_2 film [36].

Solar cells may also need an encapsulant layer above the active layer to prevent shocks and reduce corrosion. Honeycomb or moth-eye graded index structures imprinted by hot-embossing have been explored to reduce reflections from the top surface of a PVC plastic encapsulant layer [37]. The quantum efficiency of a solar cell with a graded-index encapsulant improved across the spectrum at normal incidence, resulting in a 3.3% improvement of efficiency; however, at high angles, the short-wavelength performance degraded significantly. An encapsulant that performs well at even high angles of incidence was fabricated by Yamada and colleagues. They analyzed the effect of the shape of a moth-eye structure using rigorous coupled wave simulations and fabricated an optimized coating for silicon solar cells (i.e., rounded nanocones) by nanoimprinting an acrylic resin [38]. When placed on top of a standard encapsulated silicon solar cell and deployed in Nagoaka, Japan, power output of the cell was improved by 4% at normal incidence and by up to 15% at angles as large as 80° or more. Polymer layers can also be transferred onto solar cells after being patterned. Chen and Sun transferred a nanoimprinted PMMA layer with an egg-carton structure onto a polycrystalline silicon solar cell which improved the conversion efficiency from 10.4% to 13.5% owing to substantial reduction in reflections [39].

Nanotextured encapsulants or protective surfaces can present advantages beyond light-trapping, such as superhydrophobicity for self-cleaning or antifogging. In such multi-purpose nanotextures, design tradeoffs emerge. For example, consider a periodic array of nanocones with subwavelenth spacing. The best graded index profile for antireflection is achieved through sharp tips; however, a self-cleaning surface in which water droplets readily roll off favors rounded tips to allow water droplets to stably span adjacent cones over a pocket of air. Moreover, while both photon and liquid management favor high aspect ratio structures, mechanical stability against buckling imposes additional constraints. By optimizing across all of these constraints, Park et al. [40] produced a silanized quartz structure with a cubic paraboloid profile with a center-to-center spacing of 200 nm, a height of 1.1 μm, and a tip radius of curvature of 17 nm. This structure demonstrated superhydrophobicity (contact angles >165°) and reduced reflection to light of wavelengths of 450 nm and longer across incident angles as large as 60° (Figure 4).

2.4 Summary

We have shown that nanoscale and mesoscale structures can be used to effectively reduce reflection losses from the top of solar cells. The refractive index profile of nanostructures and the spacing, height, and profile of mesostructures determine the ultimate antireflection performance. RCWA and FDTD simulation are useful tools for optimizing antireflective structures over the wavelengths and incident angles of interest. High power conversion efficiencies resulting from reduced reflections have been demonstrated for structured antireflection layers and for directly patterned active layers.

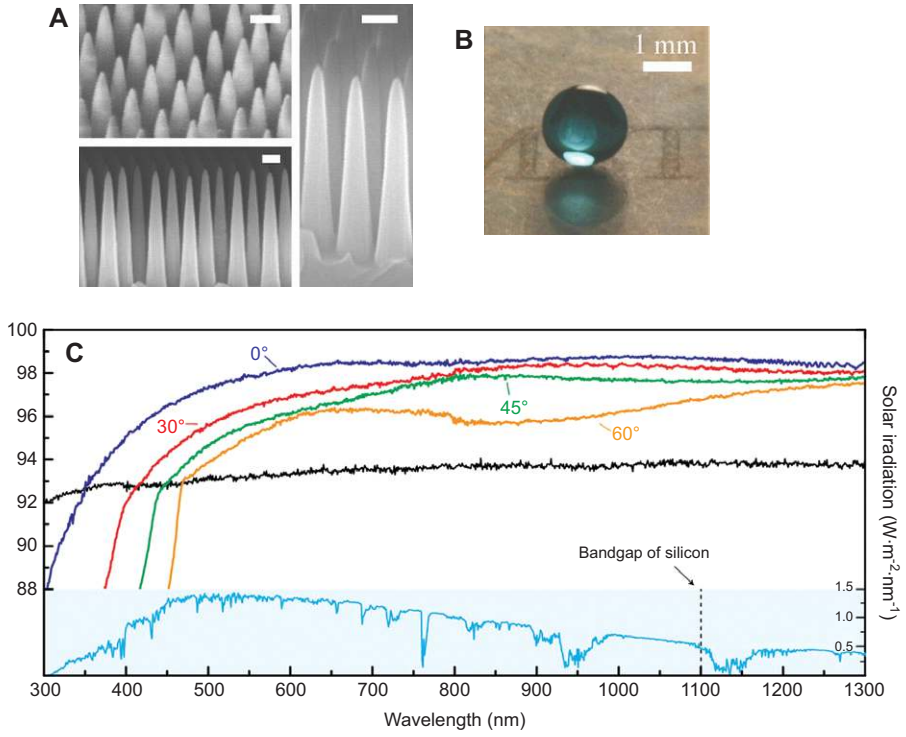

Figure 4 Cubic paraboloid nanostructure (A) SEM (scale bars=200 nm), (B) Photograph showing superhydrophobicity, and (C) transmission spectrum with solar spectrum as a reference at different angles of incidence. Adapted with permission from [39], ©2012 American Chemical Society.

3 Scattering structures and waveguides

3.1 Overview and theory

Eliminating reflections allows more light to enter a photovoltaic device; however, once inside the active layer, it must be absorbed to contribute to power generation. Therefore, a second major goal of photon management in solar cells is to improve absorption in the active layer. To examine this further, consider the expression for the absorptance of a material:

$$A=1-T=1-I_L\left(I_0\right)^{-1}=1-10^{-\alpha L}$$

where I_0 is the incident intensity, I_L is the intensity at path length L, and α is the linear absorption coefficient, which is proportional to the imaginary part of the refractive index of a material. Thus, when α is weak (e.g., near the band edge of a semiconductor), extension of the light path beyond a single pass through the depth of the material is crucial.

The path length in solar cells with absorbers thicker than the coherence length of solar light is traditionally extended by introducing a backreflector, surface roughness, scatterers, or diffraction gratings. The absorption enhancement from roughened and reflective surfaces in bulk devices (with thickness and roughness on a scale greater than the wavelength) was examined using thermodynamic and statistical ray-optics approaches by Yablonovich and Cody [41, 42] and independently by Goetzberger [43]. The upper bound for absorption enhancement calculated from these analyses is $4n^2/\sin^2(\theta)$, where n is the refractive index of the material and θ is the half angle of the light absorption cone. For absorption from a half-space and a Lambertian surface, where roughness scatters incident light isotropically, this limit reduces to the more familiar form, $4n^2$. To approach this level of enhancement, rough transparent conductive oxides [44] and substrates [45] for thin film cells have been fabricated. Periodic structures with low symmetry, such as pyramids, also act as efficient quasi-isotropic scatterers [46] and are widely used in thick crystalline silicon solar cell devices where alkaline etching of (100) wafers produces a pyramidal structure [47]. Multi-crystalline silicon cells produce facets and dimples when etched in acids and bases,

respectively [48]; these structures show some absorption enhancement.

In thin structures or in structures where the scale of the scattering texture is on the order of the wavelength of light, wave effects become important. A more general theory is therefore required to calculate the potential absorption enhancement in this case. Yu and colleagues used a statistical temporal coupled-mode theory to examine the problem [49]. In this theory, they consider an absorbing layer of thickness d that supports a number of excitable guided resonances (*M*) and a number of channels (*N*) that couple light from free space into the resonances through a periodic structure on the surface. They find that the absorption enhancement is proportional to:

$$F \propto M(Nd)^{-1}$$

Thus, enhancement can be increased by throttling the number of channels by modifying the surface structure or by reducing the thickness of the structure while maintaining the number of available resonances. They show that for surface structures with periodicity slightly smaller than the wavelengths of interest, light trapping in bulk cells can far exceed the $4n^2$ limit, but only for a narrow range of wavelengths and angles of incidence. Conversely, in ultra-thin slabs with deep subwavelength confinement, extreme absorption enhancement is achievable over a large bandwidth and a large set of angles of incidence. Similar findings were derived numerically by Bozzola and colleagues for crystalline silicon, amorphous silicon, and CIGS solar cells [50].

While the possibility of exceeding the bulk limit in the nanophotonic regime is appealing, it is worth noting that light trapping should not come at the expense of other losses in the cell. For example, the enhancement factor for an ultra-thin layer of material may be high, but the overall absorption may still be low. Also, surface structures can increase surface recombination and backside structures can interfere with high-quality thin-film growth [51].

It is clear that using a combination of surface texture and waveguiding, high light absorption enhancement can be achieved. In the following sections, we examine recent analytical and experimental progress in these areas.

3.2 Gratings and surface structures

While the general theory suggests that grating structures have a high absorption enhancement limit with appropriate periodicity ($4\pi n^2$), there has also been additional insight into how to design gratings to optimize light trapping performance [52, 53]. In general, 2D gratings perform better than 1D gratings because they couple to more resonant modes in the absorber, however both 1D and 2D gratings have been studied to show the effects of varying other parameters.

Barettin and colleagues examined the effect of placement of a 1D grating on long-wavelength absorption in dye-sensitized solar cells [54]. In this type of cell, a film of a nanocrystalline large-bandgap semiconductor (e.g., TiO_2) is coated with a dye, attached to a transparent conductive electrode, immersed in a liquid electrolyte containing a redox couple (e.g., I^-/I_3^-) , and sandwiched by another metallized counter-electrode. Light incident on the semiconductor layer produces electrons that are transferred from the photoexcited dye to the semiconductor film and out to the transparent contact while the redox couple reduces the oxidized dye, providing a transport pathway for holes through the electrolyte to the counter electrode [55]. Variants formed with different materials (including a solid-state hole transport material) [56] and nanostructures [57] have emerged to improve power conversion efficiency and stability. When placed on top of a 10 μm titania layer (i.e., on the side of the incident light), a grating with a pitch of 500 nm had a negligible effect on absorption of 700 nm light whereas a grating on the shadow side of the layer (between the semiconductor and the electrolyte) showed improved absorption of around 20%.

The work of Meng and colleagues examined the combined effect of period and placement on absorption enhancement in solar cells with gratings on both the top and bottom sides of the active layer [58]. The authors showed a simulated improvement in the short-current density of 65% by using a 2D 250 nm grating to reduce reflections at the front surface and a 2D 750 nm grating to increase the light path of long wavelengths at the back surface. Wang and colleagues from Shanui Fan's group worked with us and arrived at a similar result with respect to an optimized structure for a 2 μm equivalent thickness silicon solar cell [59]. Here, an optimized structure had a 500-nm period nanocone grating on the top of the cell and a 1000-nm period nanocone grating on the bottom. In addition, cones with a higher aspect ratio were used on the top surface to improve the antireflection effects.

The aspect ratio in tapered gratings is an interesting consideration. SangMoo Jeong, Erik Garnett, and colleagues from our group built on our silicon nanocone platform to construct hybrid polymer-silicon solar cells [60]. We found that cones with a height to diameter aspect ratio of less than two would allow the spin-coated PEDOT:PSS to fully conform to the substrate while still offering excellent optical properties. Moreover, unlike the analysis for

antireflection, which showed that taller cones were always better, the optimal aspect ratio for nanocones acting as a combined antireflection and diffraction grating is 0.9 owing to the fact that high aspect ratio structures also promote less lateral scattering within the active layer (Figure 5).

With respect to shape, gratings of low symmetry are more efficient than those of high symmetry, but the effect is only important for normally incident light [52, 53]. This can be understood because normally incident light has an even modal profile. Symmetric structures have odd and even resonant modes. The incident light can therefore couple into only half of the modes in symmetric structures.

In breaking the symmetry of a grating, it is preferable to skew the shape of the grating rather than breaking the periodicity because reflections increase in the latter case. Gjessing and colleagues performed numerical optimizations to compare various shapes of periodic backside structures for 20 μm thick crystalline silicon solar cells, including cylinders, cones, dimples, inverted pyramids, roof-mosaics, and two structures of lower symmetry named "rose" and "zigzag" [61]. The tapered structures perform better than the cylinders, and, as expected from theory, the structures with the lowest symmetry, especially the zigzag structure, are predicted to provide absorption enhancement close to the $4n^2$ limit at normal incidence (corresponding to a photocurrent density of 37.3 mA/cm^2). Interestingly, the optimal period for each of the films is approximately the same (700 nm for cylinders and ~950 nm for the other designs). For the designs with the larger period, performance suffers at larger angles because of out-coupling of light from higher diffraction orders.

Instead of grating-based coupling, some interesting work on nanostructured scattering layers has been conducted. Spinelli and colleagues [62] showed in simulations and experimentally that arrays of small cylindrical dielectric nanoparticles can effectively couple light into semiconductor substrates; silicon cylinders with a diameter of 125 nm and a height of 150 nm on a 400 nm pitch reduce integrated reflection from a silicon substrate from 32.2% to 7.5%; the effect can be further enhanced by using a silicon nitride antireflection layer. The reduced reflection is attributed to effective coupling of light into the semiconductor substrate; while both spheres and cylinders have large scattering cross-sections to interact with incident light, cylinders can couple light into the substrate through a leaky Mie resonance whereas these resonances in spheres of a similar size are essentially isolated. New resonances with more effective substrate coupling emerge in larger spheres: Grandidier and colleagues [63] proposed a light-trapping scheme based on a periodic array of wavelength-scale dielectric spheres. An array of such spheres acts as a diffraction grating but can also couple to guided modes in an absorber through coupled whispering gallery resonances in the sphere array. When placed close to adjacent spheres, the circulating resonances beneath the surface of the individual spheres couple to form so-called "jet" waveguide modes. FDTD simulations show broadband absorption enhancement owing to scattering and a doubling in absorption around the wavelength of 665 nm, which is the resonant frequency for the coupled whispering gallery mode. Shin and colleagues heterogeneously integrated p++-doped InGaAs nanowires on the rear side of a silicon solar cell via catalyst-free MOCVD growth [64]. The rest of the rear surface of the silicon was passivated with a nitride layer and the nanowires were surrounded by a metal backreflector and rear contact. It was found by analyzing direct and diffuse transmission in the heterostructure without the metal contact that the nanowires

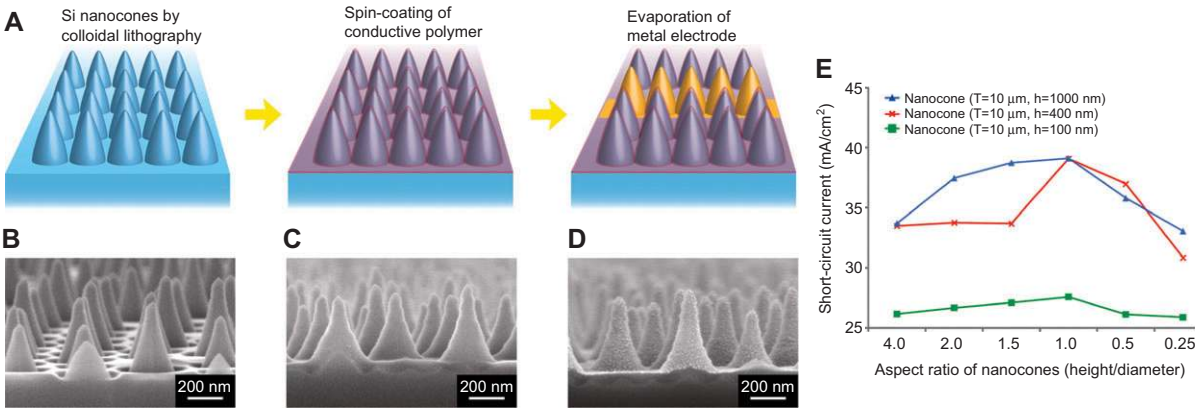

Figure 5 (A–D) Fabrication process and (E) simulated optimum aspect ratio for a hybrid polymer-silicon nanocone solar cell. Reused with permission from [59], ©2012 American Chemical Society.

scatter most light above the 950 nm wavelength diffusely. Thus, the nanowires act to scatter light at large angles which the metal contact then reflects back into the solar cell to extend the light path. In addition, the structure offers electronic advantages since it acts as a rear point contact. With only 1.5% of the silicon surface covered, the recombination at the rear surface is greatly reduced. The device with the nanowire rear contact showed a 36% improvement in power conversion efficiency as compared to a reference structure with a planar backreflector.

3.3 Waveguiding

The dramatic effects of waveguiding in ultra-thin planar layers have been shown in a number of studies. One numerical study showed that a simple 1D sinusoidal grating could increase the daily energy output of an 10 nm-thick non-tracking PV device by 60% compared to a planar structure with an optimized antireflection coating [65]. Yu and colleagues showed an average enhancement of 12 times the expected bulk limit in a 5 nm thick absorber layer surrounded by a cladding layer and a scattering layer (Figure 6). Callahan and colleagues [66] presented a local density of optical states approach to analyzing nanophotonic absorption enhancement and present a variety of techniques for achieving this goal, including a portfolio of ultra-thin waveguides (Figure 7), inhomogeneous structures, and spectral-reweighting. Munday and colleagues from the same group show a specific example: enhancement in a 10nm P3HT:PCBM layer clad on both sides by a 45 nm layer of GaP to form a high-low-high refractive index slot waveguide structure can exceed the $4n^2$ limit from 560 to 680 nm via coupling into three waveguide modes [67]. Finally, Naqavi and colleagues analyzed the case of simultaneous wavelength scale scattering and subwavelength confinement at oblique angles of incidence [68]. Interestingly, they find that light coupling at oblique angles of incidence does not significantly decrease the potential absorption improvement factor.

Light trapping in waveguide modes has also been explored in non-planar slabs. Yu and colleagues [69] showed numerically that a corrugated slab of amorphous silicon 70 nm thick sandwiched between two layers of dielectric material could absorb the same amount of light as a 400 nm thick planar film. Strong light trapping was attributed to the design which combined the antireflective effects of the dielectric material and the coupling of light into leaky resonant modes within the amorphous silicon, which allow nanostructures of various shapes to act as efficient optical antennae [70].

In another study, instead of using the nanocone architecture in the active layer of the device to promote antireflection, Zhu, Hsu, and colleagues from our group used our silica sphere coating and dry etching technique for fabricating nanocone substrates which we subsequently used as a template to grow 280 nm thin-film amorphous nanodome solar cells. The cells had 94% measured absorption in the wavelength range from 400 to 800 nm, owing to coupling into guided modes (verified through electromagnetic simulations, see Figure 8). The improvement in absorption translated into a final device efficiency of 5.9%, 25% higher than a planar control [71].

In collaboration with Bataglia and colleagues, Ching-Mei Hsu in our group expanded on this work to further optimize the structure. First, we fabricated a 270 nm-thick p-i-n cell, and a randomly textured zinc oxide front electrode deposited by low-pressure chemical vapour deposition [72]. Nanopillar, convex nanodome, and concave nanocone substrates were investigated and compared against a flat backreflector. Cells grown on the nanocone substrates demonstrated an impressive device efficiency

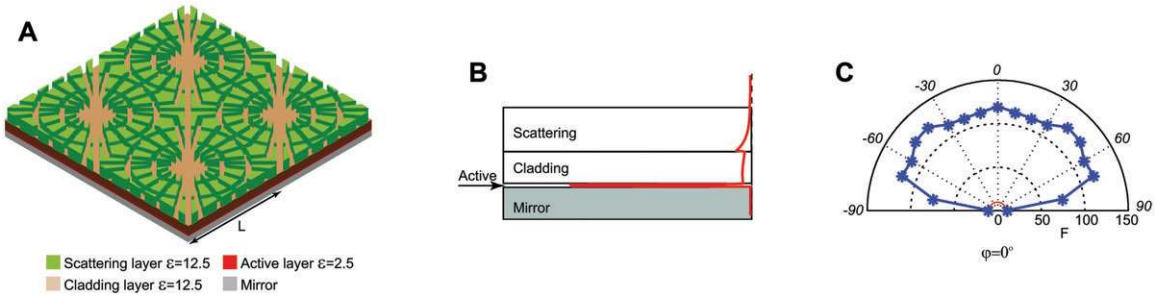

Figure 6 (A) Structure, (B) electric field intensity profile, and (C) angular-dependent enhancement factor of an ultra-thin solar cell. The $4n^2$ limit to absorption enhancement, shown in red, is far exceeded in this structure. Adapted from [48], ©2010 National Academy of Sciences.

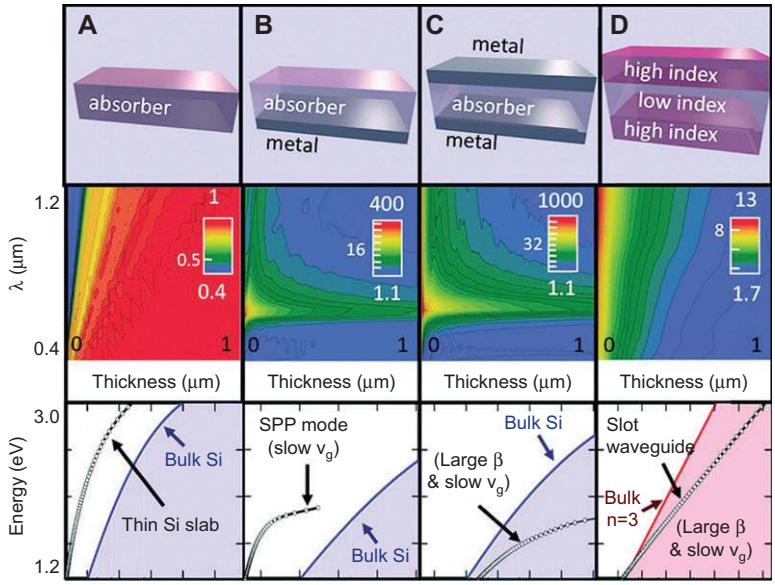

Figure 7 Potential absorption factor relative to the $4n^2$ limit for slab waveguides of different thicknesses (A) in air, (B) with a metal reflector on one side, (C) with metal reflectors on both sides, and (D) with a high-index cladding layer on both sides. Note that confinement in the layer enables absorption beyond the bulk limit. Adapted with permission from [65], ©2012 American Chemical Society.

of 9.7%, a 20% increase compared to the planar sample owing to coupling to guided optical modes. Other samples showed good light trapping properties but concomitant degradation of electrical properties. Absorption was also shown to be relatively insensitive to grating period in this case owing to the initial quasi-omnidirectional scattering from the front textured transparent contact, which results in angle-averaging of the light trapping effects of the nanocones themselves. With a slight modification to the fabrication process, the authors created a substrate with a hexagonal array of nanocavities that yielded a final amorphous silicon cell with a device efficiency of 10.9% [73], rivaling that of cells deposited on a random pyramidal textured substrate (Figure 9).

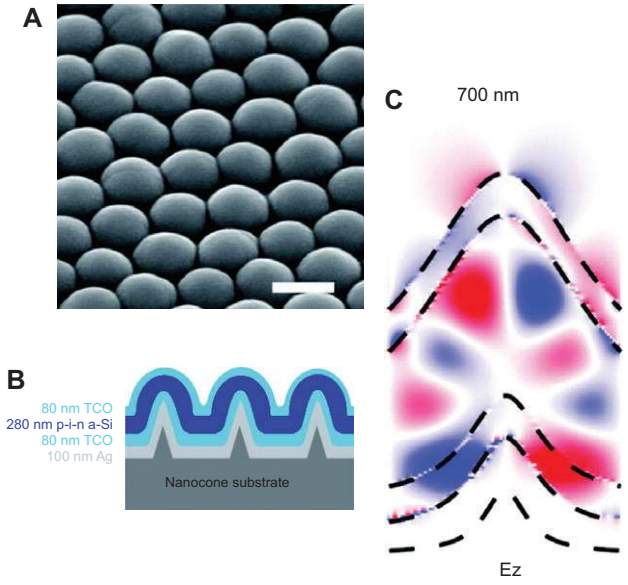

Figure 8 (A) Structure (scale bar=500 nm), (B) schematic, and (C) electromagnetic simulation of an amorphous silicon nanodome cell showing the presence of an electric field component in the vertical direction, which indicates coupling into guided modes in the active layer. Reused with permission from [70].

Using the silica nanosphere template without etching the underlying substrate, Yao, Yao, and colleagues [74] in our group developed an architecture for solar cells comprising an array of hollow shells which acts simultaneously as scattering layer and a set of spherical waveguides. The structure was fabricated by performing LPCVD coating of a silica sphere template with nano-crystalline silicon. Absorption in this structure is greatly enhanced owing to circulating guided resonances. By optimizing the balance between the internal and external leakage rates in the structure, we experimentally demonstrated up to a 20-fold absorption enhancement in an amorphous silicon film only 50 nm thick (Figure 10). We also showed excellent angular absorption performance and the ability to transfer the nanoshells to flexible substrates.

It is finally important to note that in solar cell designs with high parasitic optical losses, the benefits of light trapping structures can be severely mitigated. Consider a standard silicon solar cell with a non-ideal rear metal reflector. If the loss in the rear reflector is on the order of 5–6%, the

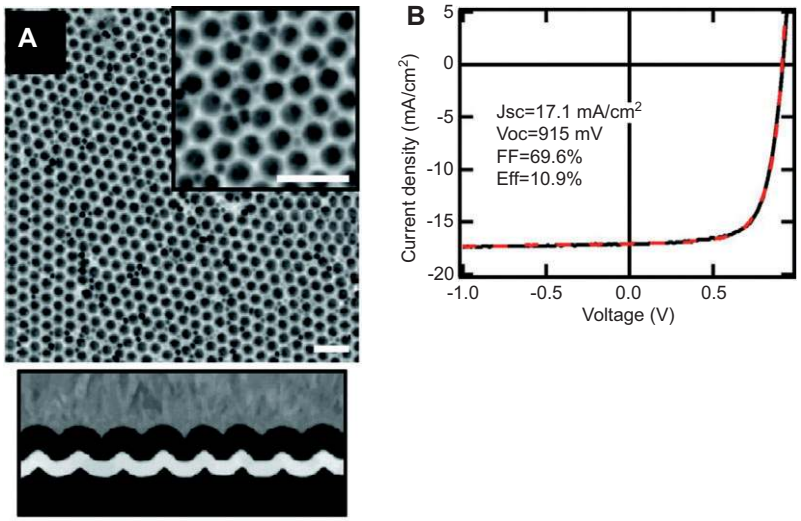

Figure 9 (A) Top and side views of an amorphous silicon solar cell grown on a nanocavity substrate (scale bars=1 μm) and (B) current/voltage curve showing comparable performance of periodic and random nanostructures. Adapted with permission from [73], ©2012 American Chemical Society.

improvement in current from enhanced light trapping could be halved [51]. This agrees with the numerical investigation by Gjessing and colleagues, in which the authors used a spacer layer between the grating and the metal backreflector. Their structure showed a larger absorption enhancement from a backside 2D grating as compared with similar designs in 2 and 5 μm silicon films owing to reduced parasitic losses. Similar conclusions were found in the study of a 2.4 μm-thick polycrystalline periodic nanodome architecture formed by electron beam evaporation and annealing of silicon on a periodically patterned sol-gel surface [75]. Light trapping in the structure was predicted to operate near the $4n^2$ limit when the cell was sandwiched between lossless transparent conductive oxide contacts. However, when typical TCO losses were taken into account in the optical model, no significant improvement was observed over conventional designs owing to parasitic absorption in the transparent contact layers. The authors suggest several techniques for improving experimental performance, including employing a planarized or highly scattering backreflector rather than a conformal back-reflector and minimizing the contact area between the transparent conductive oxide and the absorber layer in the device. It is clear that the use of metals, heavily doped semiconductors, or other lossy materials in light-trapping designs should be carefully evaluated.

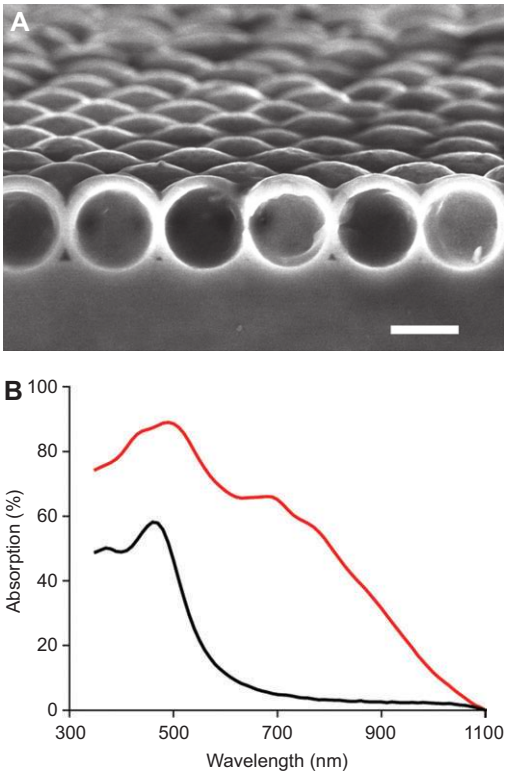

Figure 10 (A) Structure of a nanoscrystalline hollow nanoshell absorber layer (scale bar=300 nm) and (B) improved absorption performance of nanoshell (red) vs. co-deposited planar film (black). Adapted from [74].

Electrical losses from light trapping structures of different shapes was also highlighted by Vervisch and colleagues using a thin organic cell with a metal grating backreflector as an example [76]. While the carrier generation rate of an optimized cell with a grating is higher than an equivalent planar cell, the internal electric field within the organic cell is severely altered, and thus carriers are poorly harvested, resulting in an overall lower power

conversion efficiency (Figure 11). Very recently, indium phosphide nanowire p-i-n solar cells were developed with efficiencies up to 13.8%, rivaling planar cells [77]. Light absorption was optimized for wires on a given pitch (400 nm) by changing the diameter of the wires (180 nm) to maximize resonant light trapping. In modeling the electromagnetic fields in the device, much of the absorption was found to occur near the tip of the wire; the authors thus reduced the depth of the heavily doped n region to minimize electrical losses.

Given the importance of eliminating these mitigating factors, many simulation tools that couple optical and electrical performance of solar cells have emerged to evaluate potential light-trapping designs when used in a full cell design [76, 78, 79]. Experimental techniques have also been developed to extract non-parasitic absorption from luminescence experiments [80] and to probe the quantum efficiency of guided modes directly [81].

3.4 Summary

The study of absorption enhancement benefits from a rich set of general theory and simulation tools to optimize the geometry (placement of structures, period, aspect ratio, and shape), and thus the optical properties of light trapping surface structures and waveguide absorbers. Designs with efficiencies rivaling or exceeding conventional architectures have been demonstrated by our group and others. Materials selection and optimization of fabrication techniques is required to achieve simultaneously high absorption, small parasitic losses, and strong electrical properties in solar cells.

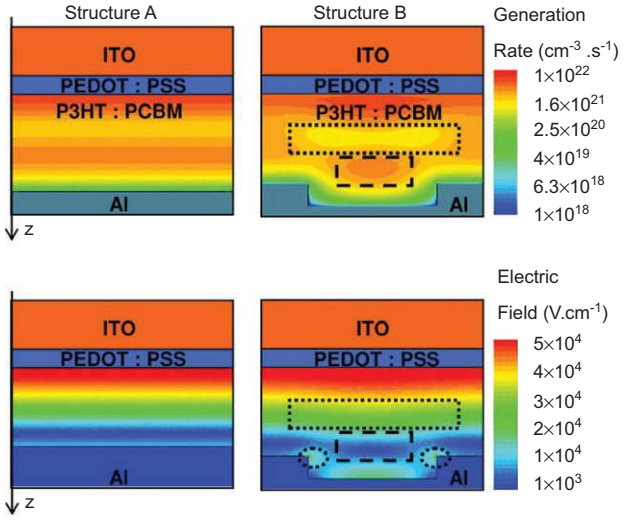

Figure 11 Generation rate and electric field distribution for planar and grating-based organic solar cells. Used with permission from [76].

4 Photonic crystals

4.1 Overview and theory

While eliminating reflection and enhancing absorption are central to achieving low-cost, high efficiency solar cells, devices may have a host of other requirements for photon management architectures in real applications. For example, solar cells in building-integrated photovoltaics may need to be partially transparent, those in concentrator systems may require directional selectivity, and those in thermophotovoltaic systems require optical layers with specifically tuned absorption and emission spectra. For these needs, photonic crystals could offer an excellent solution.

Photonic crystals enable control of light propagation just as atomic crystals enable control of electron conduction [82]. In an atomic crystal, the periodic arrangement of atoms results in a spatially periodic electrical potential on the scale of electron waves. Electrons with certain energies and momenta will be able to pass through the crystal without scattering while other combinations of energies and momenta will be forbidden. Similarly, photonic crystals present a varying dielectric potential through the spatial arrangement of materials with different dielectric permittivity on the scale of the wavelength of light. When the dielectric contrast and scaling of features in the structure is properly selected, the structure presents either a complete photonic bandgap (i.e., no propagating waves in any direction) or a partial gap/stop-band (i.e., no propagating waves in certain directions) in a band of frequencies.

In the following sections, we explore a number of properties of photonic crystals useful to photon management. First, we look at photonic crystal reflectors placed on the shadow side of the active layer of a solar cell or in an intermediate layer in a multi-junction device. Here, photonic crystals provide wavelength-selective near-perfect reflection, scattering, or interfacial modes for increasing the light path. We then look at absorbers and emitters which are themselves structured as photonic crystal slabs, which demonstrate field localization for enhanced absorption. Finally, we look at front-side photonic crystals used for antireflection, directional selectivity, and coupling of incident light to interfacial modes.

4.2 Photonic crystal reflectors

Perhaps the simplest photonic crystal structure is an alternating periodic stack of layers with different dielectric permittivity. Assuming negligible absorption and proper scaling of the layers, light propagation through the layers is forbidden, and the structure becomes a near perfect reflector to the light frequencies within the photonic band gap. A key advantage of photonic crystals when compared to traditional metallic reflectors or highly scattering back reflectors is tunable spectral selectivity, which allows near-perfect reflectivity inside the band gap and high transmissivity outside the bandgap. In addition, near the red edge of the photonic crystal bandgap, strong light localization can occur in the high refractive index layers of the stack, potentially further enhancing absorption [83]. Such 1-D photonic crystals, also known as Distributed Bragg Reflectors, have been heavily investigated for solar cells.

One useful application for wavelength-selective photonic crystal reflectors is for semi-transparent building-integrated photovoltaics (BIPV). BIPV are used for roofs, skylights, windows, or facades in place of traditional building materials to generate electricity while simultaneously providing thermal management and tinting/shading.

Semi-transparent amorphous silicon (a-Si) solar cell modules have been deployed in BIPV systems at a New York City subway station [84] and on the façade of a building in Korea [85]. a-Si is an attractive material for BIPV applications owing to its availability, relative non-toxicity, compatibility for deposition over large areas, and low temperature coefficient. However, its thickness must be minimized in order to maintain a high electric field across the active layer and minimize light-induced degradation [4]. O'Brien and colleagues [86] analyzed a DBR rear electrical contact for a superstrate-configuration a-Si BIPV. The structure comprised alternating silica nanoparticle and sputtered ITO layers adjacent to a 100 nm-thick a-Si absorber. Simulations using the scattering matrix method showed that a DBR with a Bragg reflection peak centered around 600 nm would provide nearly identical short-circuit current to an optimized zinc oxide/silver contact while transmitting over 40% of incoming sunlight, which would be available for building heating and cooling. The authors also proposed an optimized architecture to provide sufficient transmission for indoor lighting by re-centering the reflection band of the DBR around 500 nm and deposited amorphous silicon layers atop DBRs with different reflection bands to demonstrate color control of transmitted light.

A full a-Si cell with photonic crystal reflectors was fabricated by Kuo and colleagues [87]. Here, a stack of three TiO_2/SiO_2 DBRs with different stop bands were deposited behind the ZnO back contact of an amorphous silicon solar cell; by tuning the position of the stop bands of the three reflectors, the authors improved the efficiency of an amorphous silicon solar cell with a 200 nm thick absorbing layer from 3.68% to 4.66% while allowing transparency in the 450 nm wavelength region, resulting in blue light transmission through the cell (Figure 12).

Other BIPV-compatible cells with DBRs were made from organic photovoltaics. In an organic solar cell, bound electron-hole pairs (excitons) are formed by incident light and separated at a heterojunction interface between a donor and acceptor polymer. By choosing particular donor and acceptor materials, for example chloroaluminum phthalocyanine and fullerene (C_{60}), a cell can be made to absorb light in the infrared and ultraviolet while maintaining transparency in the visible. A TiO_2/SiO_2 DBR reflector was sputtered onto the backside of such an organic device to reflect 99% of incident light in the wavelength range of 695–910 nm [88]. When used with a 120 nm thick ITO back transparent contact and a backside antireflection layer for visible light, efficiency was increased to 1.5% compared to 1.0% in a device without a reflector. In addition to improving power generation in the device, the authors note that the DBR could be used for simultaneous near-infrared rejection in architectural cooling applications. As an alternative to sputtering, spin coated DBRs have also been explored as a low-cost, low deposition temperature reflector in organic cells [89].

Dye-sensitized solar cells (DSCs) have also been cited for their potential in building integrated photovoltaics [90]. In addition to being partially transparent, photonic crystal reflectors in dye cells must be permeable to the hole

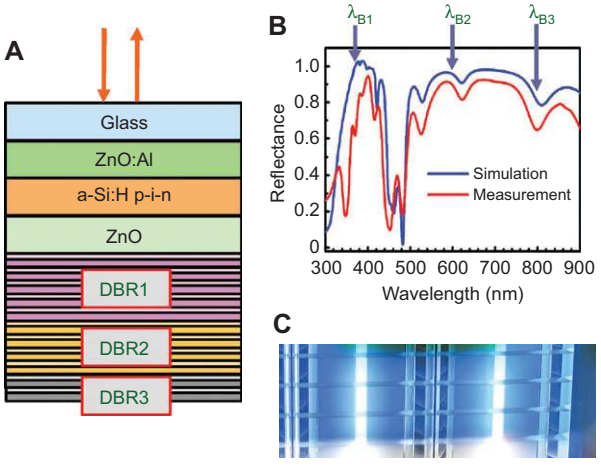

Figure 12 (A) Schematic, (B) reflection spectrum, and (C) photograph of transmitted light for an amorphous silicon solar cell backed by a stack of three DBRs. Used with permission from [86].

transport electrolyte. Porous DBRs comprising alternating layers of spin-cast SiO_2 and TiO_2 particles have been demonstrated to improve the power conversion efficiency of a DSC from 3.9% for a reference cell to 4.6%. The photocurrent is greatly enhanced by the DBR while the photovoltage, angular performance, and transparency of the device are preserved [91]. Optimizing the overlap between the photonic bandgap and the absorption band of the dye and the thickness of active layer (and thus the number of available photonic states for light coupling) gives rise to a larger enhancement of the photocurrent. DBRs have also been integrated seamlessly into columnar TiO_2 electrodes for dye cells using periodic current pulsing of a titanium plate [92]. The electrodes were then peeled off and inserted into a dye cell. The space between the columns allows for penetration of the electrolyte. The power conversion efficiency of these devices was improved from 3.66% to 5.61%; further optimizations led to an even higher efficiency of 7.11%.

In addition to reflectivity generated by a photonic band-gap, scattering or coupling to waveguide modes may be desired from photonic crystal reflectors. Zeng and colleagues [93] fabricated a crystalline silicon solar cell on top of a 675 μm-thick silicon wafer; one-dimensional gratings with a 1.1 μm period were patterned on the backside through projection photolithography and etching, and DBRs were deposited by plasma-enhanced chemical vapour deposition. The DBR was designed to have strong reflectivity in the wavelength range from 800 to 1100 nm, while the grating was designed to diffract incident light at these wavelengths well beyond the critical angle for total internal reflection in silicon. The authors found that the photonic crystal and grating together performed better than the grating alone, improving overall efficiency from 11.1% to 13.2%. Further, the angular performance of the devices is impressive; 80% of power efficiency enhancement is preserved even through incident angles as high as 45° owing to the preservation of the reflection properties of the photonic crystal bandgap and the diffraction properties of the gratings at large angles. Short circuit current enhancement of 19% was observed by another group [94] in a thinner 5 μm device. Note that unlike planar DBRs, where more layers improve the photonic crystal performance, simulations show that for DBRs with integrated gratings, parasitic losses due to grating coupling to guided modes within the DBR instead of the active layer could degrade performance [95].

Another way to introduce scattering to photonic crystals is to use structures of higher dimensionality. O'Brien and colleagues studied photoconductivity enhancement in absorber layers using opaline photonic crystal backreflectors [96]. Opals consist of a hexagonally-close packed array of spheres in three dimensions. The photonic band structure of opals does not contain a wide photonic bandgap but instead has a narrow stopgap in the [1 1 1] crystal direction. The authors deposited a 40-layer thick opal of glass spheres on the back side of a 254 nm thick amorphous silicon film. Peaks in absorption enhancement in the a-Si films corresponded well with scalar wave approximation simulations, and the authors found through FDTD simulations that absorption enhancement arose both from backreflection in the stop band and from diffraction from the opaline structure into guided modes at the interface between the opal and the absorber, including a defect mode that exists within the photonic stop gap (the surface of a 3 dimensional crystal, which is a break in the crystal periodicity, can be considered a defect).

The inverse of the opal structure has also been investigated. Inverse opals are fabricated by backfilling the void space between the spheres of an opaline structure and selectively etching, dissolving, or calcining the sphere template.

Inverse TiO_2 opals with interconnected cavities have been heavily investigated for dye-sensitized solar cells. Early investigations focused on replacing the nc-TiO_2 film with an inverse opal photonic crystal [97–101]. Any gains from nanophotonic effects in these designs were mitigated by a greatly reduced surface area for dye loading compared to nanoscrytalline thin films, volume contraction and cracking of the inverse opals during removal of the sphere template, or because incident light within the stopband of the crystal was rejected and therefore not absorbed by the dye inside the inverse opal. Instead, inverse opals were found to be most effective when coupled to a nc-TiO_2 thin film, i.e., a bilayer DSC structure. Halaoui et al. [102] showed an improvement in the incident photon-to-electron conversion efficiency in a bilayer DSC structure over either the planar layer of nanoscrystalline TiO_2 or a photonic crystal TiO_2 backbone alone. Similarly, Guldin et al. [103] and colleagues observed improved short circuit current density in a non-optimized bilayer DSC. Lee and coworkers [104] improved the power conversion efficiency of a bilayer DSC device to 8.3% compared to 6.5% for a comparable reference cell with the same dye loading. They found the improvement to be highly dependent on the optical coupling between the photonic crystal and the thin film. Li and colleagues [105] found similar levels of improvement in relative efficiency in a recent study (an improvement of 2.76% to 3.59%). Different mechanisms for absorption enhancement in inverse opals coupled to thin films have been elucidated, including backreflection from the photonic band gap, the localization of heavy photons at the edges of the photonic gap (a narrow-band

effect which enhances light absorption in the red regime) [106], enhanced backscattering due to disordered regions in the crystal [102], and, significantly, because of the localization of light in the absorber film due to multiple resonant modes at the interface between the crystal and the absorber [107].

It should also be noted that inverse opals can be used even on devices with more exotic morphologies. Mihi and colleagues developed a technique to transfer an inverse opal from a silica coated substrate to another surface by encapsulating it in a polymer, undercutting it with hydrofluoric acid, transferring it, and dissolving the polymer. Using this technique, they formed a porous TiO_2 inverse opal electrode and transferred it onto a nanowire dye-sensitized solar cell (Figure 13). The authors improved the efficiency of the solar cell from 0.586% to 0.679%, demonstrating the optical quality of the transferred film [108].

Instead of or in addition to being used at the back side of a solar cell, photonic crystals reflectors have also been investigated as intermediate layers in multi-junction solar cells. The current through a the series connection in a multi-junction cell is limited by the junction with the lowest current, and thus current matching is critical to achieving high efficiency in these devices. In addition to band-gap and device engineering approaches, intermediate reflectors could be used to tune absorption in each junction.

For example, consider an amorphous-silicon/microcrystalline silicon tandem solar cell (micromorph solar cell). The thickness of the top amorphous layer in such a cell is restricted because of the hole diffusion length; therefore, current matching is difficult to achieve by changing the thickness of the sub-cells. Bielawny and colleagues [109] simulated photonic crystals as intermediate reflectors in micromorph cells using the Fourier modal method. Simulated optimized 1D and 3D photonic crystal structures provide 20% and 30% higher current, respectively, in the amorphous silicon top cell of a tandem device over a standard cell. While the 1D structure demonstrates a strong 0th order reflection band, the 3D structure is also capable of diffraction to higher order modes, further increasing the light path.

The same group fabricated devices with an inverse-opal 3D structure on the top cell [110] and in a full tandem device [111]. The authors use a superstrate configuration with the active layers deposited atop a textured transparent conductive oxide to take advantage of scattering at the front interface. The dip-coated PMMA opal template is applied next. While the spheres assemble amorphously on the rough surface, they form a crystalline opal structure in the upper layers of the stack. Atomic layer deposition of aluminum-doped zinc oxide is used to backfill the opal to form a conductive inverse opal. The PMMA template is then dissolved, and the back layers of the tandem cell (the microcrystalline silicon bottom cell and back contact) are deposited. In the fabricated device, the upper cell performance increases near the reflection band of the photonic crystal while the performance of the bottom cell degrades significantly owing to the properties of light propagation through the inverse opal as well as electrical and reflection losses at the interface between the photonic crystal and the μc-Si layer. Introducing a thin (90 nm) ZnO index matching layer below the photonic crystal has been proposed to limit deleterious reflections at longer wavelengths; simulations have shown that the absorption loss in the bottom cell can be partially recovered through this technique [112].

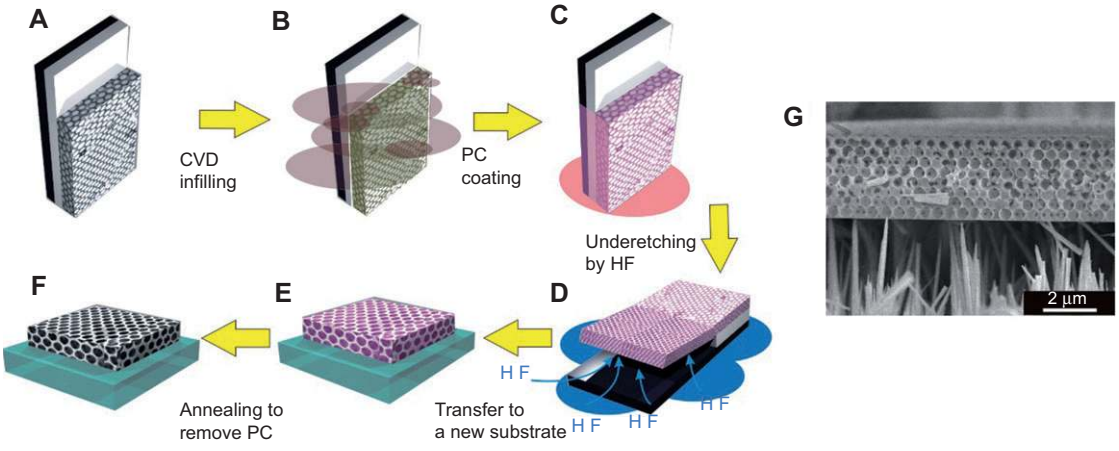

Figure 13 Transfer process and final structure of an inverse-opal framework for a dye-sensitized solar cell. Used with permission from [108].

1D photonic crystal intermediate reflectors with integrated rectangular and triangular surface diffraction gratings were simulated by another group [113]. An optimized structure with triangular gratings had 77 % simulated absorption (400–1100 nm) in the top cell and transmission of 41% (1100–1800 nm) to the bottom cell. The signature of light trapping imparted by the photonic crystal was a band-edge absorption enhancement factor of 4.6 in the wavelength range of 867–1100 nm. The group also demonstrated a fabricated structure grown by plasma enhanced chemical vapor deposition (PECVD), electron beam (E-beam) lithography, and dry etching.

Beyond controlling the flux of incident light into each layer in a multi-junction cell, DBRs are also being explored to manage photons generated by radiative recombination and reabsorbed in each layer, i.e., photon recycling. Photon recycling plays an important role in high-efficiency materials, for example III-V semiconductors, where non-radiative recombination pathways for photogenerated carriers are minimized. For example, Miller and colleagues [114] have performed calculations which show that a single-junction 3 μm gallium arsenide cell is theoretically capable of achieving an efficiency of 33.2%, close to that predicted by the detailed balance limit for a single junction device (33.5%); however, if the back-reflector for such a cell leaks 20% of photons, the overall efficiency drops by 1.3%. Surprisingly, this is not primarily due to a loss of incident photons (the short-circuit photocurrent from the device drops only 0.2%) but instead to a loss of photons generated through radiative recombination in the active layer (which manifests as a drop in the open-circuit voltage of the device). This is consistent with a thermodynamic argument: if some photons are not recycled, the carrier product of electrons and holes (np) drops, which in turn reduces the splitting of the quasi-Fermi energies of the exited populations in the device and thus the open circuit voltage [45, 115].

Several III-V cells with high photon recycling could be connected through tunnel junctions to form a multi-junction device; such solar cells are currently the highest efficiency photovoltaic devices available [1]. Leakage of recycled photons from one sub-cell to other parts of the device would result in a decreased photovoltage from that sub-cell and an overall decrease in efficiency. Photonic crystal reflectors with an appropriate stop-band could therefore be used to maximize voltage while a complementary technique, such as bandgap engineering, could be used to balance current. In recent work, Garcia and colleagues [116] used the transfer matrix method to calculate the effect of an optimized DBR on the GaAs subcell of a triple junction device. The authors considered several materials which could be epitaxially grown on GaAs and provide near-isotropic high reflectance around GaAs's band edge of 880 nm. The authors describe a technique to optimize the thickness and number of repeats of a DBR intermediate reflector for recycled photons and discuss a multi-section DBR with each section optimized to a particular propagation angle to approximate isotropic reflection. The maximum calculated reflectivity achievable for a single GaAs cell is 88% while that for the GaAs middle cell of a triple-junction device is 83%.

Finally, there has been some theoretical work to compare the relative merits of different types of photonic crystals for backreflecting applications. Bermel and colleagues compared the simulated optical performance of several different photonic crystal architectures, including DBRs, DBRs with 1D and 2D gratings, 2D photonic crystal slabs, 3D woodpile crystals, and inverse opals in a 2 μm c-Si solar cell [117]. When optimized, the structures all were predicted to demonstrate between 24% and 32% absorption enhancement over a device with an aluminum backreflector. DBRs with 2D gratings with different grating periods had the highest enhancement since the grating periods could be tuned independently to avoid strongly overlapping modes and broaden the frequency response. The work also established the superiority of triangular lattice slabs over square lattice slabs as backreflectors owing to a bandstructure with a larger stopband for one polarization of light and a slower group velocity for light in this structure.

4.3 Photonic crystal absorbers

Another property of photonic crystals important to light trapping is localization of light within the photonic crystal itself. This effectively tailors the absorption spectrum of a material by enhancing the path length or residence time of light at certain frequencies. Forming absorbers which are themselves structured as photonic crystals has thus been an area of active interest. One system that lends itself well to this design is the organic solar cell. The absorption length and the exciton diffusion length in such devices typically differ by an order of magnitude (100s vs. 10s of nm, respectively [118]); strong light absorption in thinner layers of the active material, particularly in wavelengths close to the infrared absorption edge, are desired. An early theoretical study [119] describes photonic crystal Bloch mode absorbers in organic solar cells comprising donor (P3HT) nanowires in an acceptor (PCBM) slab. Through FDTD simulations, the authors theorized a 35.6% absorption enhancement by optimizing the periodicity (500 nm),

wire diameter (400 nm), and slab thickness (150 nm). Near the absorption edge, this structure provides a high density of Bloch modes, two Bloch modes for coupling normally incident light, and long modal lifetime owing to low group velocity (slowly propagating light) in the dispersion relation at the relevant wavelengths (600–700 nm). While absorption could be effectively enhanced in such a bilayer structure, the donor and acceptor are separated on a length scale incommensurate with efficient exciton diffusion.

A light trapping strategy compatible with the bulk heterojunction architecture, in which donor and acceptor polymers phase-separate into an intimately intermixed nanostructure, involves impressing a low-index photonic crystal, for example, nanocrystalline zinc oxide or titanium dioxide ridges, pillars, or cones, into a bulk-heterojunction matrix. In addition, this approach offers higher index contrast than the case where the polymers alone are used as the photonic crystal materials. 1D and 2D periodic impressed OPV absorbers have been studied theoretically in a number of works [120–122]. Plane-wave transfer and scattering matrix simulations [120] showed absorption enhancements of 17% of an optimized ridge/pillar photonic crystal solar cell over an optimized planar structure of equivalent volume. Simulations also place a lower bound of 0.3 on the difference in refractive index needed in the low-index layer to give rise to enhanced absorption with P3HT:PCBM. Other simulations [121] revealed a reduction of the distance between exciton creation and separation, suggesting favorable electrical properties in addition to higher absorption. Tapered structures in the low-index layer, such as cones and pyramids, are predicted to outperform rectangular structures owing to antireflection effects and, in some configurations, higher exciton generation close to the interface between the polymer and the top contact [122].

The modal character of the enhancement was also analyzed [120] by comparing peaks in the absorption profile and the photonic band structure of the absorber layer. Both broad-band and narrow-band modes exist with short and long lifetimes, respectively. Further, not all modes result in absorption enhancement (i.e., some are optically inactive). The importance of an active spacer or flash layer, i.e., a thin planar layer of the polymer blend sitting on one side of the photonic crystal, is highlighted in this and another study [123]. Light is concentrated in quasiguided modes at the bottom face of a photonic crystal slab; without a spacer layer, light trapping would occur in the electrode material rather than the active layer and result in negligible absorption enhancement.

Ko and colleagues fabricated organic solar cells with a photonic crystal active layer [124] by patterning the low-efficiency TDPTD:PCBM system with a soft, non-wetting perfluoropolyether mold to form a hexagonal array of columns with a height of 180 nm and a periodicity of 400 nm. The columns were back-filled with 5 nm nc-ZnO particles; the thickness of the layer was tuned to provide both index contrast in the photonic crystal and an optical spacing layer for interference effects. The device showed higher absorption than a comparable planar device at wavelengths higher than 600 nm, with a maximum absorption enhancement of 3.5X at 660 nm over a comparable planar device. Moreover, the photonic crystal cell's incident photon-to-electron conversion efficiency is improved over the entire spectrum, not merely in the region of enhanced absorption, owing both to light concentration in the absorbing layers and improved internal quantum efficiency, perhaps through enhanced electrical performance from chain or grain alignment [125–128] or due to modification of the exciton creation and dissociation profile. Photonic crystal devices were on-average 68% more efficient than planar counterparts, albeit on modestly performing <1% efficient devices. Recently, the same group conducted studies on both standard and inverted organic solar cells [129]. In the P3HT:PCBM materials system with a copper phthalocyanine layer, up to a 90% absorption enhancement and a 13% efficiency enhancement were observed in photonic crystal devices, producing a device with a record efficiency at the time of 2.91%.

Crystalline silicon and amorphous silicon photonic crystal slabs consisting of stripes [130–132], nanopillars/rods [31, 133], nanowells/nanoholes [130, 134–136], tapered columns [137], and conical nanowells [138] have been investigated theoretically and experimentally for solar cell applications. All of these studies found large improvements in absorption and/or short circuit current density as a result of coupling to quasi-guided modes in the slab. This is consistent with the theory of Yu and colleagues [49], which showed that inclusions of low index material in a high index absorber layer can significantly improve absorption. However, passivation of etched structures and other electrical problems remain challenges to increasing conversion efficiency of devices using patterned silicon photonic crystal slabs in practice.

Many of the photon management approaches described here use periodic photonic crystals. However, quasi-periodic and disordered systems could also be of interest [139]. For example, a 2D photonic crystal slab of silicon was simulated with different degrees of disorder [140]. It was found that slab where the center-to-center distance was randomized around a mean value of 20% of

the lattice spacing performed best; smeared Bloch resonances were still visible in the absorption spectrum of this structure. Structures with too much disorder, where Anderson-type localization dominates, do not perform as well. Another study on a random set of circular holes in a 100 nm a-Si film confirmed this finding [141]. The disordered 2D slab showed up to five-fold integrated absorption enhancement compared to an unpatterned planar structure. Interestingly, structures with periodic vs. completely random patterns perform almost identically, while an amorphous hole array, i.e., where short-range correlations are present with no long range order, enhance absorption most strongly.

The use of photonic crystal slabs to tailor the absorption spectrum of a film could also be used for the reciprocal purpose of tailoring its emission spectrum. This technique has particular utility for an emerging class of solar energy converters based on thermophotovoltaics (TPV). In this type of system, higher energy photons from sunlight are concentrated and absorbed by a material in order to raise its temperature; the absorber's spectrum is such that emissivity at longer wavelengths is suppressed in order to prevent re-emission. The absorber is thermally coupled to a narrowband emitter that is closely matched to the absorption of a low-bandgap semiconductor solar cell. The goal of the TPV system is therefore to convert the broadband nearly black-body spectrum of the sun to a narrow band spectrum well matched to a solar cell. The theoretical efficiency of such a system is ~85%. Photonic crystals that could function both as selective, temperature stable absorbers and emitters [142–145] for TPV applications, as well as for photon management within the PV diode itself [146] are currently being investigated.

4.4 Front-side photonic crystals

Front-side photonic crystals also have unique light-trapping properties in some types of solar cells. For example, in ultra-thin absorber layers, a new physical mechanism for light absorption enhancement using DBRs emerges. In [147], the authors propose forming a DBR from ITO and ATO layers in the front transparent conducting electrode. Unlike the previous studies we have discussed, the DBR is not used as a back reflector. The organic P3HT:PCBM active layer is positioned between the ITO/ATO layers and the back metal contact. Given its refractive index, the organic layer essentially becomes the back layer of the photonic crystal if its thickness is properly scaled (in this case, to 40 nm). Thus, at the interface between the organic layer and the metal, Optical Tamm Plasmons may be formed [148]. Unlike surface plasmon polaritons, Optical Tamm Plasmons can be directly excited from the air (i.e., they have wavevectors that lie inside the light cone) by both polarizations of light. The authors calculate a maximum 35% improvement in absorption in this structure when only two periods of the photonic crystal are present. The authors confirm that the absorption enhancement is the same regardless of incident polarization and show a peak in the field at the metal/organic interface, providing evidence for enhancement by Optical Tamm Modes (Figure 14).

An aperiodic dieletric stack was investigated as a front-side coating for an ultra-thin 15 nm CuPc:PCTBI organic solar cell in [149]. Such a stack would ideally act as an antireflective coating at short wavelengths and as a high-reflectivity mirror at long wavelengths, where the organic cell absorbs poorly. The authors present an analytic approach to calculate the improvement in short

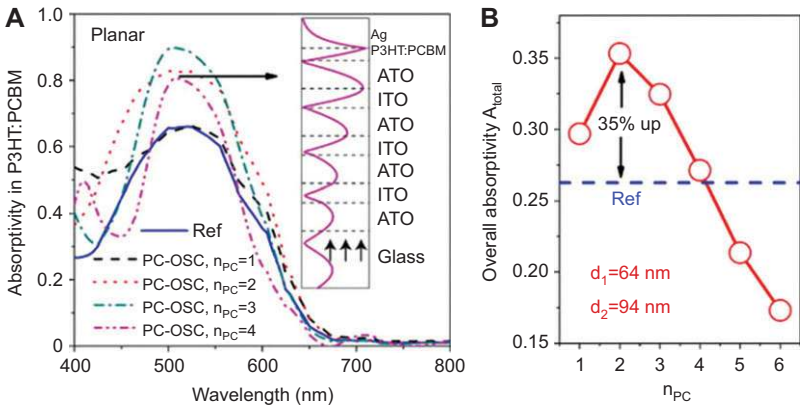

Figure 14 (A) Absorption spectra and field amplitude and (B) integrated absorption as a function of number of photonic crystal periods for an Optical-Tamm based light trapping scheme. Used with permissionfrom [147].

circuit current density for physically realizable values of reflection amplitude and phase and then use a numerical optimization technique to design multi-layer dielectric stacks that exhibit these properties. Averaged over a full day (i.e., over a range of incident angles), with an optimized 4-layer structure, the authors calculate a potential 40% improvement in short-circuit current density for an ultra-thin 15 nm bilayer organic solar cell and 32% for a bulk heterojunction device.

Ulbrich and colleagues present a design for front-side photonic crystals which exploit directional selectivity to enhance performance [150]. The principle of this structure is to place a selective filter at the front of the solar cell over top of a randomized scattering layer. The filter accepts only direct and circumsolar sunlight and rejects photons incident at oblique angles. Therefore, light enters the cell at a narrow range of angles, is randomly scattered by a textured surface and thus trapped outside the exit cone of the filter (thus modifying the θ term in the $4n^2/\sin^2(\theta)$ bulk limit). The light path can be theoretically enhanced by up to a factor of 26,000 times in silicon for light entering at incident angles <2.5° off normal. The filter can also be designed to operate only below a certain threshold frequency such that diffuse light from higher, more readily absorbed frequencies is allowed to pass. The authors propose two types of photonic crystals to implement directional selectivity; a TiO_2/SiO_2 Rugate filter, which is a stack of dielectric materials with a continuously varying refractive index profile, and an inverse opal structure with an incomplete band gap. The filters are shown to be effective only when light is normally incident on the cell throughout the day, i.e., in solar energy systems which track the sun. In non-tracking systems, no improvement is expected. The authors demonstrate an improvement in absorptance near the band edge in a 37 μm silicon slab using a commercial Rugate filter and calculate 5% and 7.5% annual improvement in energy yield from 1 μm silicon cells implementing optimized Rugate and inverse opal filters, respectively.

Finally, front-side photonic structures could also be used to reduce thermodynamic losses associated with radiative recombination. The entropy of light spontaneously emitted from the active layer is much larger than that of light incident from the sun owing to the larger solid angle of the emission cone. Polman and Atwater show that limiting the emission cone, and thus the entropy of the emitted light, could improve the open circuit voltage of a solar cell by up to 315 mV at room temperature and thus push solar cell efficiencies much closer to the theoretical thermodynamic maximum [151].

4.5 Summary

We have shown that photonic crystals have been investigated in many classes of thin-film solar cells. Photonic crystals are particularly well-suited for photon management in applications where spectral and directional selectivity or light localization could minimize photon loss while maintaining other properties, such as transparency, angular performance, or porosity. While some studies have demonstrated efficiency enhancement, only theoretical gains have been predicted for many applications. To realize the full potential of photonic crystals in practice, continued effort to refine fabrication techniques and to seek structures with better electrical properties is essential.

5 Conclusion

In this article, we have reviewed the rich physics underlying nano and meso-scale structures for light management in solar cells. Such structures enable excellent antireflection, large absorption enhancement, and the possibility to tailor the optical response of solar cells for various applications in unprecedented ways. Nanoscale photon management structures have shown real efficiency gains in many types of photovoltaic devices, but simulation, characterization, and improved fabrication techniques are important for ensuring that improved optical performance does not come at the expense of electrical properties in order for these structures to contribute to the widespread adoption of future generations of solar cells.

Acknowledgements: This review is based in part on work supported by the Center on Nanostructuring for Efficient Energy Conversion (CNEEC) at Stanford University, an Energy Frontier Research Center funded by the U.S. Department of Energy, Office of Science and Office of Basic Energy Sciences under Award Number DE-SC0001060.

Received January 18, 2013; accepted March 4, 2013

References

[1] Green MA, Emery K, Hishikawa Y, Warta W, Dunlop ED. Solar cell efficiency tables (version 39). Prog Photovoltaics Res Appl 2012;20(1):12–20.

[2] Barbose G, Wiser R. Tracking the Sun V. Berkeley, CA: Lawrence Berkeley National Laboratory; 2012.

[3] Candelise C, Winskel M, Gross R. Implications for CdTe and CIGS technologies production costs of indium and tellurium scarcity. Prog Photovoltaics Res Appl 2012;20(6):816–31.

[4] Shimizu T. Staebler-Wronski effect in hydrogenated amorphous silicon and related alloy films. Jpn J Appl Phys 2004;43(6A):3257–68.

[5] Peumans P, Bulovic V, Forrest SR. Efficient photon harvesting at high optical intensities in ultrathin organic double-heterostructure photovoltaic diodes. Appl Phys Lett 2000;76(19):2650–2.

[6] Mattos LS, Scully SR, Syfu M, Olson E, Yang L, Ling C, Kayes BM, He G, Devices A, Clara S. New module efficiency record: 23.5% under 1-sun illumination using thin-film single-junction GaAs solar cells. In 2012 38th IEEE Photovoltaic Specialists Conference (PVSC). 2012, 3187–90.

[7] Gu M, Ouyang Z, Jia B, Stokes N, Chen X, Fahim N, Li X, Ventura MJ, Shi Z. Nanoplasmonics: a frontier of photovoltaic solar cells. Nanophotonics 2012;1(3)–(4):235–48.

[8] Catchpole KR, Polman A. Plasmonic solar cells. Opt Express 2008;16(26):21793–800.

[9] Stephens RB, Cody GD. Optical reflectance and transmission of a textured surface. Thin Solid Films 1977;45(1):19–29.

[10] Southwell WH. Antireflection index matching on optical surfaces. J Opt Soc Am 1991;8(3):549–53.

[11] Poitras D, Dobrowolski JA. Toward perfect antireflection coatings. 2. Theory. Appl Optics 2004;43(6):1286–95.

[12] Xi J-Q, Schubert MF, Kim JK, Schubert EF, Chen M, Lin S-Y, Liu W, Smart JA. Optical thin-film materials with low refractive index for broadband elimination of Fresnel reflection. Nat Photonics 2007;1(3):176–9.

[13] Chhajed S, Schubert MF, Kim JK, Schubert EF. Nanostructured multilayer graded-index antireflection coating for Si solar cells with broadband and omnidirectional characteristics. Appl Phys Lett 2008;93(25):251108.

[14] Yan X, Poxson DJ, Cho J, Welser RE, Sood AK, Kim JK, Schubert EF. Enhanced omnidirectional photovoltaic performance of solar cells using multiple-discrete-layer tailored- and low-refractive index anti-reflection coatings. Adv Funct Mater 2012;23(5):583–90.

[15] Koynov S, Brandt MS, Stutzmann M. Black nonreflecting silicon surfaces for solar cells. Appl Phys Lett 2006;88(20):203107.

[16] Branz HM, Yost VE, Ward S, Jones KM, To B, Stradins P. Nanostructured black silicon and the optical reflectance of graded-density surfaces. Appl Phys Lett 2009;94(23):231121.

[17] Chyan JY, Hsu WC, Yeh JA. Broadband antireflective poly-Si nanosponge for thin film solar cells. Opt Express 2009;17(6):4646–51.

[18] Oh J, Yuan H-C, Branz HM. An 18.2%-efficient black-silicon solar cell achieved through control of carrier recombination in nanostructures. Nat Nanotechnol 2012;7(Sept):743–8.

[19] Lee Y-J, Ruby DS, Peters DW, McKenzie BB, Hsu JWP. ZnO nanostructures as efficient antireflection layers in solar cells. Nano Letters 2008;8(5):1501–5.

[20] Wu T-H, Chuang RW, Huang C-Y, Cheng C-Y, Huang C-Y, Lin Y-C, Su Y-K. ZnO nanoneedles/ZnO:Al film stack as an anti-reflection layer for high efficiency triple junction solar cell. Electrochem Solid State Lett 2012;15(6):H208–10.

[21] Diedenhofen SL, Grzela G, Haverkamp E, Bauhuis G, Schermer J, Rivas JG. Broadband and omnidirectional anti-reflection layer for III/V multi-junction solar cells. Sol Energ Mat Sol Cells 2012;101:308–14.

[22] Garnett E, Yang P. Light trapping in silicon nanowire solar cells. Nano Letters 2010;10(3):1082–7.

[23] Zhu J, Yu Z, Burkhard GF, Hsu C-M, Connor ST, Xu Y, Wang Q, McGehee M, Fan S, Cui Y. Optical absorption enhancement in amorphous silicon nanowire and nanocone arrays. Nano Letters 2009;9(1):279–82.

[24] Srivastava SK, Kumar D, Singh PK, Kar M, Kumar V, Husain M. Excellent antireflection properties of vertical silicon nanowire arrays. Sol Energ Mat Sol Cells 2010;94(9):1506–11.

[25] Yu Z, Gao H, Wu W, Ge H, Chou SY. Fabrication of large area subwavelength antireflection structures on Si using trilayer resist nanoimprint lithography and liftoff. J Vac Sci Technol B Microelectron Nanometer Struct 2003;21(6):2874.

[26] Huang Y-F, Chattopadhyay S, Jen Y-J, Peng C-Y, Liu T-A, Hsu Y-K, Pan C-L, Lo H-C, Hsu C-H, Chang Y-H, Lee C-S, Chen K-H, Chen L-C. Improved broadband and quasi-omnidirectional anti-reflection properties with biomimetic silicon nanostructures. Nat Nanotechnol 2007;2(12):770–4.

[27] Hsu C-M, Connor ST, Tang MX, Cui Y. Wafer-scale silicon nanopillars and nanocones by Langmuir-Blodgett assembly and etching. Appl Phys Lett 2008;93(13):133103–9.

[28] Jeong S, Hu L, Lee HR, Garnett E, Choi JW, Cui Y. Fast and scalable printing of large area monolayer nanoparticles for nanotexturing applications. Nano Letters 2010;10(8):2989–94.

[29] Song YM, Bae SY, Yu JS, Lee YT. Closely packed and aspect-ratio-controlled antireflection subwavelength gratings on GaAs using a lenslike shape transfer. Opt Letters 2009;34(11):1702–4.

[30] Forberich K, Dennler G, Scharber MC, Hingerl K, Fromherz T, Brabec CJ. Performance improvement of organic solar cells with moth eye anti-reflection coating. Thin Solid Films 2008;516(20):7167–70.

[31] Alaeian H, Atre AC, Dionne JA. Optimized light absorption in Si wire array solar cells. J Opt 2012;14(2):024006.

[32] Deinega A, Valuev I, Potapkin B, Lozovik Y. Minimizing light reflection from dielectric textured surfaces. J Opt Soc Am A 2011;28(5):770–7.

[33] Dobrowolski JA, Poitras D, Ma P, Vakil H, Acree M. Toward perfect antireflection coatings: numerical investigation. Appl Optics 2002;41(16):3075–83.

[34] Fan Z, Kapadia R, Leu PW, Zhang X, Chueh Y-L, Takei K, Yu K, Jamshidi A, Rathore AA, Ruebusch DJ, Wu M, Javey A. Ordered arrays of dual-diameter nanopillars for maximized optical absorption. Nano Letters 2010;10(10):3823–7.

[35] Jeong S, McDowell M, Cui Y. Low-temperature self-catalytic growth of tin oxide nanocones over large areas. ACS Nano 2011;5(7):5800–7.

[36] Ho W-J, Ou S-H, Lee Y-Y, Liu J-J. Broadband wavelength and wide-acceptance angle of the SiO2 sub-wavelength surface structure for solar cells using CF4 reactive ion etching. Thin Solid Films 2013;529:257–62.

[37] Han K-S, Lee H, Kim D, Lee H. Fabrication of anti-reflection structure on protective layer of solar cells by hot-embossing method. Sol Energ Mat Sol Cells 2009;93(8):1214–7.
[38] Yamada N, Kim ON, Tokimitsu T, Nakai Y, Masuda H. Optimization of anti-reflection moth-eye structures for use in crystalline silicon solar cells. Prog Photovoltaics Res Appl 2011;19(2):134–40.
[39] Chen JY, Sun KW. Enhancement of the light conversion efficiency of silicon solar cells by using nanoimprint anti-reflection layer. Sol Energ Mat Sol Cells 2010;94(3):629–33.
[40] Park K-C, Choi HJ, Chang C-H, Cohen RE, McKinley GH, Barbastathis G. Nanotextured silica surfaces with robust superhydrophobicity and omnidirectional broadband supertransmissivity. ACS Nano 2012;6(5):3789–99.
[41] Yablonovitch E, Cody GD. Intensity enhancement in textured optical sheets for solar cells. IEEE T Electron Dev 1982;29(2):300–5.
[42] Yablonovitch E. Statistical ray optics. J Opt Soc Am 1982;72(7):899–907.
[43] Goetzberger A. Optical confinement in thin Si-solar cells by diffuse back reflectors. In Proceedings of the 15th IEEE Photovoltaics Specialists Conference; 1981, p. 867.
[44] Berginski M, Hüpkes J, Schulte M, Schöpe G, Stiebig H, Rech B, Wuttig M. The effect of front ZnO:Al surface texture and optical transparency on efficient light trapping in silicon thin-film solar cells. J Appl Phys 2007;101(7):074903.
[45] Sato K, Gotoh Y, Hayashi Y, Adachi K, Naishimura H. Reports Res. Lab. Asahi Glass Co. Ltd. 1992;40:129.
[46] Nelson J. The physics of solar cells. London: Imperial College Press; 2003.
[47] Zhao J, Wang A, Altermatt PP, Wenham SR, Green MA. 24% Efficient perl silicon solar cell: Recent improvements in high efficiency silicon cell research. Sol Energ Mat Sol Cells 1996;42:87–99.
[48] Macdonald DH, Cuevas A, Kerr MJ, Samundsett C, Ruby D, Winderbaum S, Leo A. Texturing industrial multicrystalline silicon solar cells. Sol Energy 2004;76(1)–(3):277–83.
[49] Yu Z, Raman A, Fan S. Fundamental limit of nanophotonic light trapping in solar cells. Proc Natl Acad Sci USA 2010;107(41):17491–6.
[50] Bozzola A, Liscidini M, Andreani LC. Photonic light-trapping versus Lambertian limits in thin film silicon solar cells with 1D and 2D periodic patterns. Opt Express 2012;20(Suppl 2): A224–44.
[51] Mokkapati S, Catchpole KR. Nanophotonic light trapping in solar cells. J Appl Phys 2012;112(10):101101.
[52] Yu Z, Raman A, Fan S. Fundamental limit of light trapping in grating structures. Opt Express 2010;18(53):A366–80.
[53] Han SE, Chen G. Toward the Lambertian limit of light trapping in thin nanostructured silicon solar cells. Nano Letters 2010;10(11):4692–6.
[54] Barettin D, Di Carlo A, De Angelis R, Casalboni M, Prosposito P. Effect of dielectric Bragg grating nanostructuring on dye sensitized solar cells. Opt Express 2012;20(Suppl 6) (Nov):A888–97.
[55] O'Regan B, Grätzel M. A low-cost, high-efficiency solar cell based on dye-sensitized colloidal TiO2 films. Nature 1991;353(6346):737–40.
[56] Hardin BE, Snaith HJ, McGehee MD. The renaissance of dye-sensitized solar cells. Nat Photonics 2012;6(3):162–9.
[57] Tétreault N, Grätzel M. Novel nanostructures for next generation dye-sensitized solar cells. Energy Environ Sci 2012;5(9):8506–16.
[58] Meng X, Drouard E, Gomard G, Peretti R, Fave A, Seassal C. Combined front and back diffraction gratings for broad band light trapping in thin film solar cell. Opt Express 2012;20(Suppl 5) (May):A560–71.
[59] Wang KX, Yu Z, Liu V, Cui Y, Fan S. Absorption enhancement in ultrathin crystalline silicon solar cells with antire-flection and light-trapping nanocone gratings. Nano Letters 2012;12(3):1616–9.
[60] Jeong S, Garnett EC, Wang S, Yu Z, Fan S, Brongersma ML, McGehee MD, Cui Y. Hybrid silicon nanocone-polymer solar cells. Nano Letters 2012;12(6):2971–6.
[61] Gjessing J, Sudbø AS, Marstein ES. Comparison of periodic light-trapping structures in thin crystalline silicon solar cells. J Appl Phys 2011;110(3):033104.
[62] Spinelli P, Verschuuren MA, Polman A. Broadband omnidi-rectional antireflection coating based on subwavelength surface Mie resonators. Nat Commun 2012;3:692.
[63] Grandidier J, Callahan DM, Munday JN, Atwater HA. Light absorption enhancement in thin-film solar cells using whispering gallery modes in dielectric nanospheres. Adv Mater (Deerfield Beach, Fla.) 2011;23(10):1272–6.
[64] Shin JC, Mohseni PK, Yu KJ, Tomasulo S, Montgomery KH, Lee ML, Rogers JA, Li X. Heterogeneous integration of InGaAs nanowires on the rear surface of si solar cells for efficiency enhancement. ACS Nano 2012;6(12):11074–9.
[65] Wang P, Menon R. Simulation and analysis of the angular response of 1D dielectric nanophotonic light-trapping structures in thin-film photovoltaics. Opt Express 2012;20(Suppl 4) (July):A545–53.
[66] Callahan DM, Munday JN, Atwater HA. Solar cell light trapping beyond the ray optic limit. Nano Letters 2012;12(1):214–8.
[67] Munday JN, Callahan DM, Atwater HA. Light trapping beyond the 4n2 limit in thin waveguides. Appl Phys Lett 2012;100(12):121121.
[68] Naqavi A, Haug F, Battaglia C, Herzig H, Ballif C. Light trapping in solar cells at the extreme coupling limit. J Opt Soc Am B 2013;30(1):13–20.
[69] Yu Y, Ferry VE, Alivisatos AP, Cao L. Dielectric core-shell optical antennas for strong solar absorption enhancement. Nano Letters 2012;12(7):3674–81.
[70] Cao L, Fan P, Vasudev AP, White JS, Yu Z, Cai W, Schuller JA, Fan S, Brongersma ML. Semiconductor nanowire optical antenna solar absorbers. Nano Letters 2010;10(2):439–45.
[71] Zhu J, Hsu C-M, Yu Z, Fan S, Cui Y. Nanodome solar cells with efficient light management and self-cleaning. Nano Letters 2010;10(6):1979–1984.
[72] Hsu C-M, Battaglia C, Pahud C, Ruan Z, Haug F-J, Fan S, Ballif C, Cui Y. High-efficiency amorphous silicon solar cell on a periodic nanocone back reflector. Adv Energy Mater 2012;2(6):628–33.
[73] Battaglia C, Hsu C-M, Söderström K, Escarré J, Haug F-J, Charrière M, Boccard M, Despeisse M, Alexander DTL, Cantoni M, Cui Y, Ballif C. Light trapping in solar cells: can periodic beat random? ACS Nano 2012;6(3):2790–7.
[74] Yao Y, Yao J, Narasimhan VK, Ruan Z, Xie C, Fan S, Cui Y. Broadband light management using low-Q whispering gallery modes in spherical nanoshells. Nat Commun 2012;3:664.

[75] Lockau D, Sontheimer T, Becker C, Rudigier-Voigt E, Schmidt F, Rech B. Nanophotonic light trapping in 3-dimensional thin-film silicon architectures. Opt Express 2013;21(51):A42–52.
[76] Vervisch W, Rivière G, Vedraine S, Biondo S, Torchio P, Duché D, Simon J-J, Escoubas L. Optical-electrical simulation of organic solar cells: Influence of light trapping by photonic crystal and ZnO spacer on electrical characteristics. J Appl Phys 2012;111(9):094506.
[77] Wallentin J, Anttu N, Asoli D, Huffman M, Åberg I, Magnusson MH, Siefer G, Fuss-Kailuweit P, Dimroth F, Witzigmann B, Xu HQ, Samuelson L, Deppert K, Borgström MT. InP nanowire array solar cells achieving 13.8% efficiency by exceeding the ray optics limit. Science 2013;339:1057–60.
[78] Li X, Hylton NP, Giannini V, Lee K, Ekins-daukes NJ, Maier SA. Multi-dimensional modeling of solar cells with electromagnetic and carrier transport calculations. Prog Photovoltaics Res Appl 2012;21(1):109–20.
[79] Ferry VE, Polman A, Atwater HA. Modeling light trapping in nanostructured solar cells. ACS Nano 2011;5(12):10055–64.
[80] Trupke T, Daub E, Würfel P. Absorptivity of silicon solar cells obtained from luminescence. Sol Energ Mat Sol Cells 1998;53:103–14.
[81] Dissanayake DMNM, Ashraf A, Pang Y, Eisaman MD. Guided-mode quantum efficiency: A novel optoelectronic characterization technique. Rev Sci Instrum 2012;83(11):114704.
[82] Joannopoulos J, Johnson S, Winn J, Meade R. Photonic crystals: molding the flow of light (Second Edition). Princeton, NJ: Princeton University Press, 2008.
[83] Deparis O, El Daif O. Optimization of slow light one-dimensional Bragg structures for photocurrent enhancement in solar cells. Opt Lett 2012;37(20):4230–2.
[84] Pagliaro M, Ciriminna R, Palmisano G. BIPV: merging the photovoltaic with the construction industry. Prog Photovoltaics Res Appl 2010;18(1):61–72.
[85] Yoon J-H, Song J, Lee S-J. Practical application of building integrated photovoltaic (BIPV) system using transparent amorphous silicon thin-film PV module. Sol Energy 2011;85(5):723–33.
[86] O'Brien PG, Chutinan A, Mahtani P, Leong K, Ozin GA, Kherani NP. Selectively transparent and conducting photonic crystal rear-contacts for thin-film silicon-based building integrated photovoltaics. Opt Express 2011;19(18):17040–52.
[87] Kuo MY, Hsing JY, Chiu TT, Li CN, Kuo WT, Lay TS, Shih MH. Quantum efficiency enhancement in selectively transparent silicon thin film solar cells by distributed Bragg reflectors. Opt Express 2012;20(56):A828–35.
[88] Lunt RR, Bulovic V. Transparent, near-infrared organic photovoltaic solar cells for window and energy-scavenging applications. Appl Phys Lett 2011;98(11):113305.
[89] Sun YC, Ng A, Fung MK, Djurišić AB, Chan WK. Enhancement of polymer solar cell performance using spin-coated reflector structure. Mater Chem Phys 2012;135(2–3):1044–7.
[90] Yoon S, Tak S, Kim J, Jun Y, Kang K, Park J. Application of transparent dye-sensitized solar cells to building integrated photovoltaic systems. Build Environ 2011;46(10):1899–904.
[91] Colodrero S, Mihi A, Häggman L, Ocaña M, Boschloo G, Hagfeldt A, Míguez H. Porous one-dimensional photonic crystals improve the power-conversion efficiency of dye-sensitized solar cells. Adv Mater 2009;21(7):764–70.
[92] Yip CT, Huang H, Zhou L, Xie K, Wang Y, Feng T, Li J, Tam WY. Direct and seamless coupling of TiO2 nanotube photonic crystal to dye-sensitized solar cell: a single-step approach. Adv Mater (Deerfield Beach, Fla.) 2011;23(47):5624–8.
[93] Zeng L, Yi Y, Hong C, Liu J, Feng N, Duan X, Kimerling LC, Alamariu BA. Efficiency enhancement in Si solar cells by textured photonic crystal back reflector. Appl Phys Lett 2006;89(11):111111.
[94] Zeng L, Bermel P, Yi Y, Alamariu BA, Broderick KA, Liu J, Hong C, Duan X, Joannopoulos J, Kimerling LC. Demonstration of enhanced absorption in thin film Si solar cells with textured photonic crystal back reflector. Appl Phys Lett 2008;93(22):221105.
[95] Sheng X, Johnson SG, Broderick LZ, Michel J, Kimerling LC. Integrated photonic structures for light trapping in thin-film Si solar cells. Appl Phys Lett 2012;100(11):111110.
[96] O'Brien PG, Kherani NP, Zukotynski S, Ozin GA, Vekris E, Tetreault N, Chutinan A, John S, Mihi A, Míguez H. Enhanced photoconductivity in thin-film semiconductors optically coupled to photonic crystals. Adv Mater 2007;19(23):4177–82.
[97] Huisman C. The application of inverse titania opals in nanostructured solar cells. Sol Energ Mat Sol Cells 2004;85:115–24.
[98] Somani PR, Dionigi C, Murgia M, Palles D, Nozar P, Ruani G. Solid-state dye PV cells using inverse opal TiO2 films. Sol Energ Mat Sol Cells 2005;87(1)–(4):513–9.
[99] Kwak ES, Lee W, Park N-G, Kim J, Lee H. Compact inverse-opal electrode using non-aggregated TiO2 nanoparticles for dye-sensitized solar cells. Adv Funct Mater 2009;19(7):1093–9.
[100] Liu L, Karuturi SK, Su LT, Tok AIY. TiO2 inverse-opal electrode fabricated by atomic layer deposition for dye-sensitized solar cell applications. Energy Environ Sci 2011;4(1):209–15.
[101] Seo YG, Woo K, Kim J, Lee H, Lee W. Rapid fabrication of an inverse opal TiO2 photoelectrode for DSSC using a binary mixture of TiO2 nanoparticles and polymer microspheres. Adv Funct Mater 2011;21(16):3094–103.
[102] Halaoui LI, Abrams NM, Mallouk TE. Increasing the conversion efficiency of dye-sensitized TiO2 photoelectrochemical cells by coupling to photonic crystals. J Phys Chem B 2005;109(13):6334–42.
[103] Guldin S, Hüttner S, Kolle M, Welland ME, Müller-Buschbaum P, Friend RH, Steiner U, Tétreault N. Dye-sensitized solar cell based on a three-dimensional photonic crystal. Nano Letters 2010;10(7):2303–9.
[104] Lee S-HA, Abrams NM, Hoertz PG, Barber GD, Halaoui LI, Mallouk TE. Coupling of titania inverse opals to nanocrystalline titania layers in dye-sensitized solar cells. J Phys Chem B 2008;112(46):14415–21.
[105] Li H, Tang Q, Cai F, Hu X, Lu H, Yan Y, Hong W, Zhao B. Optimized photonic crystal structure for DSSC. Sol Energy 2012;86(11):3430–7.
[106] Nishimura S, Abrams N, Lewis BA, Halaoui LI, Mallouk TE, Benkstein KD, Van de Lagemaat J, Frank AJ. Standing wave enhancement of red absorbance and photocurrent in dye-sensitized titanium dioxide photoelectrodes coupled to photonic crystals. J Am Chem Soc 2003;125(20):6306–10.

[107] Mihi A, Míguez H. Origin of light-harvesting enhancement in colloidal-photonic-crystal-based dye-sensitized solar cells. J Phys Chem B 2005;109(33):15968–76.
[108] Mihi A, Zhang C, Braun PV. Transfer of preformed three-dimensional photonic crystals onto dye-sensitized solar cells. Angewandte Chemie (International ed. in English) 2011;50(25):5712–5.
[109] Bielawny A, Rockstuhl C, Lederer F, Wehrspohn RB. Intermediate reflectors for enhanced top cell performance in photovoltaic thin-film tandem cells. Opt Express 2009;17:8439–46.
[110] Bielawny A, Üpping J, Miclea PT, Wehrspohn RB, Rockstuhl C, Lederer F, Peters M, Steidl L, Zentel R, Lee S-M, Knez M, Lambertz A, Carius R. 3D photonic crystal intermediate reflector for micromorph thin-film tandem solar cell. Physica Status Solidi (a) 2008;205(12):2796–810.
[111] Upping J, Bielawny A, Wehrspohn RB, Beckers T, Carius R, Rau U, Fahr S, Rockstuhl C, Lederer F, Kroll M, Pertsch T, Steidl L, Zentel R. Three-dimensional photonic crystal intermediate reflectors for enhanced light-trapping in tandem solar cells. Adv Mater (Deerfield Beach, Fla.) 2011;23(34):3896–900.
[112] Fahr S, Rockstuhl C, Lederer F. Sandwiching intermediate reflectors in tandem solar cells for improved photon management. Appl Phys Lett 2012;101(13):133904.
[113] Mutitu JG, Shi S, Chen C, Creazzo T, Barnett A, Honsberg C, Prather DW. Thin film silicon solar cell design based on photonic crystal and diffractive grating structures. Opt Express 2008;16(19):15238–48.
[114] Miller OD, Yablonovitch E, Kurtz SR. Strong internal and external luminescence as solar cells approach the Shockley–Queisser limit. IEEE J Photovoltaics 2012;2(3):303–11.
[115] Ross RT. Some thermodynamics of photochemical systems. J Chem Phys 1967;46(12):4590–3.
[116] Garcia I, Geisz J, Steiner M, Olson J, Friedman D, Kurtz S, García I. Design of semiconductor-based back reflectors for high Voc monolithic multijunction solar cells. In 2012 38th IEEE Photovoltaic Specialists Conference (PVSC). 2012. p. 2042–7.
[117] Bermel P, Luo C, Zeng L, Kimerling LC, Joannopoulos JD. Improving thin-film crystalline silicon solar cell efficiencies with photonic crystals. Opt Express 2007;15(25):16986–7000.
[118] Coakley KM, McGehee MD. Conjugated polymer photovoltaic cells. Chem Mater 2004;16(23):4533–42.
[119] Duché D, Escoubas L, Simon J-J, Torchio P, Vervisch W, Flory F. Slow bloch modes for enhancing the absorption of light in thin films for photovoltaic cells. Appl Phys Lett 2008;92(19):193310.
[120] Tumbleston JR, Ko D-H, Samulski ET, Lopez R. Electrophotonic enhancement of bulk heterojunction organic solar cells through photonic crystal photoactive layer. Appl Phys Lett 2009;94(4):043305.
[121] Tumbleston JR, Ko D-H, Samulski ET, Lopez R. Absorption and quasiguided mode analysis of organic solar cells with photonic crystal photoactive layers. Opt Express 2009;17(9):7670–81.
[122] Chen L, Sha WEI, Choy WCH. Light harvesting improvement of organic solar cells with self-enhanced active layer designs. Opt Express 2012;20(7):8175–85.
[123] Duché D, Drouard E, Simon J, Escoubas L, Torchio P, Le Rouzo J, Vedraine S. Light harvesting in organic solar cells. Sol Energ Mat Sol Cells 2011;95:S18–S25.
[124] Ko D-H, Tumbleston JR, Zhang L, Williams S, DeSimone JM, Lopez R, Samulski ET. Photonic crystal geometry for organic solar cells. Nano Letters 2009;9(7):2742–6.
[125] Hlaing H, Lu X, Hofmann T, Yager KG, Black CT, Ocko BM. Nanoimprint-induced molecular orientation in semiconducting polymer nanostructures. ACS Nano 2011;5(9):7532–8.
[126] Shih CF, Hung KT, Wu JW, Hsiao CY, Li WM. Efficiency improvement of blended poly(3-hexylthiophene) and 1-(3-methoxycarbonyl)-propyl-1-phenyl-(6,6)C[sub 61] solar cells by nanoimprinting. Appl Phys Lett 2009;94(14):143505.
[127] Lee JH, Kim DW, Jang H, Choi JK, Geng J, Jung JW, Yoon SC, Jung H-T. Enhanced solar-cell efficiency in bulk-heterojunction polymer systems obtained by nanoimprinting with commercially available AAO membrane filters. Small (Weinheim an der Bergstrasse, Germany) 2009;5(19):2139–43.
[128] Chou W-Y, Chang J, Yen C-T, Tang F-C, Cheng H-L, Chang M-H, Lien-Chung Hsu S, Chen J-S, Lee Y-C. Nanoimprinting-induced efficiency enhancement in organic solar cells. Appl Phys Lett 2011;99(18):183108.
[129] Ko D-H, Tumbleston JR, Schenck W, Lopez R, Samulski ET. Photonic crystal geometry for organic polymer:fullerene standard and inverted solar cells. J Phys Chem C 2011;115(10):4247–54.
[130] Meng X, Depauw V, Gomard G, El Daif O, Trompoukis C, Drouard E, Jamois C, Fave A, Dross F, Gordon I, Seassal C. Design, fabrication and optical characterization of photonic crystal assisted thin film monocrystalline-silicon solar cells. Opt Express 2012;20(Suppl 4) (May):A465–75.
[131] Park Y, Drouard E, El Daif O, Letartre X, Fave A, Kaminski A, Lemiti M, Seassal C, De Lyon U, De Lyon N. Insa-ecl-ucbl UMRC-. Absorption enhancement using photonic crystals for silicon thin film solar cells. 2009;17(16):14312–21.
[132] Zanotto S, Liscidini M, Andreani LC. Light trapping regimes in thin-film silicon solar cells with a photonic pattern. Opt Express 2010;18(5):4260–74.
[133] Chutinan A, Kherani NP, Zukotynski S. High-efficiency photonic crystal solar cell architecture. Opt Express 2009;17(11):8871–8.
[134] Mallick SB, Agrawal M, Wangperawong A, Barnard ES, Singh KK. Ultrathin crystalline-silicon solar cells with embedded photonic crystals Ultrathin crystalline-silicon solar cells with embedded photonic crystals. 2012;053113:1–4.
[135] Meng X, Gomard G, El Daif O, Drouard E, Orobtchouk R, Kaminski A, Fave A, Lemiti M, Abramov A, Roca i Cabarrocas P, Seassal C. Absorbing photonic crystals for silicon thin-film solar cells: Design, fabrication and experimental investigation. Sol Energ Mat Sol Cells 2011;95:S32–8.
[136] Han SE, Chen G. Optical absorption enhancement in silicon nanohole arrays for solar photovoltaics. Nano Letters 2010;10(3):1012–5.
[137] Malekmohammad M, Soltanolkotabi M, Erfanian A, Asadi R, Bagheri S, Zahedinejad M, Khaje M, Naderi MH. Broadband photonic crystal antireflection. J Eur Opt Soc – Rapid publications 2012;7.
[138] Du QG, Kam CH, Demir HV, Yu HY, Sun XW. Enhanced optical absorption in nanopatterned silicon thin films with a nano-cone-hole structure for photovoltaic applications. Opt Letters 2011;36(9):1713–5.

[139] Ricciardi A, Pisco M, Cutolo A, Cusano A, O'Faolain L, Krauss T, Castaldi G, Galdi V. Evidence of guided resonances in photonic quasicrystal slabs. Phys Rev B 2011;84(8):1–4.
[140] Oskooi A, Favuzzi PA, Tanaka Y, Shigeta H, Kawakami Y, Noda S. Partially disordered photonic-crystal thin films for enhanced and robust photovoltaics. Appl Phys Lett 2012;100(18):181110.
[141] Vynck K, Burresi M, Riboli F, Wiersma DS. Disordered optical modes for photon management. arXiv:1202.4601v1 2012;1–8.
[142] Rephaeli E, Fan S. Absorber and emitter for solar thermo-photovoltaic systems to achieve efficiency exceeding the Shockley-Queisser limit. Opt Express 2009;17(17):15145–59.
[143] Yeng YX, Ghebrebrhan M, Bermel P, Chan WR, Joannopoulos JD, Soljačić M, Celanovic I. Enabling high-temperature nanophotonics for energy applications. Proc Natl Acad Sci USA 2012;109(7):2280–5.
[144] Arpin KA, Losego MD, Braun PV. Electrodeposited 3D tungsten photonic crystals with enhanced thermal stability. Chem Mater 2011;23(21):4783–8.
[145] Araghchini M, Yeng YX, Jovanovic N, Bermel P, Kolodziejski LA, Soljacic M, Celanovic I, Joannopoulos JD. Fabrication of two-dimensional tungsten photonic crystals for high-temperature applications. J Vac Sci Technol B Microelectronics Nanometer Struct 2011;29(6):061402.
[146] Shemeya C, Vandervelde TE. Comparison of photonic-crystal-enhanced thermophotovoltaic devices with and without a resonant cavity. J Electron Mater 2012;41(5):928–34.
[147] Zhang X-L, Song J-F, Li X-B, Feng J, Sun H-B. Optical Tamm states enhanced broad-band absorption of organic solar cells. Appl Phys Lett 2012;101(24):243901.
[148] Kaliteevski M, Iorsh I, Brand S, Abram R, Chamberlain J, Kavokin A, Shelykh I. Tamm plasmon-polaritons: possible electromagnetic states at the interface of a metal and a dielectric Bragg mirror. Phys Rev B 2007;76(16):165415.
[149] Agrawal M, Peumans P. Broadband optical absorption enhancement through coherent light trapping in thin-film photovoltaic cells. Opt Express 2008;16(8):5385–96.
[150] Ulbrich C, Fahr S, Üpping J, Peters M, Kirchartz T, Rockstuhl C, Wehrspohn R, Gombert A, Lederer F, Rau U. Directional selectivity and ultra-light-trapping in solar cells. Physica Status Solidi (a) 2008;205(12):2831–43.
[151] Polman A, Atwater HA. Photonic design principles for ultrahigh-efficiency photovoltaics. Nat Mater 2012;11(3):174–7.